Loss of ErbB3 redirects Integrin β1 from early endosomal recycling to secretion in extracellular vesicles

Dorival Mendes Rodrigues-Junior[#*1]; Ana Rosa Saez-Ibanez[#1]; Takeshi Terabayashi[3]; Nina Daubel[2]; Taija Makinen[2]; Olof Idevall-Hagren[4]; Aristidis Moustakas[1]; Ingvar Ferby[*1,2]

[1]Department of Medical Biochemistry and Microbiology, Science for Life Laboratory, Box 582, Biomedical Center, Uppsala University, SE-751 23 Uppsala, Sweden.

[2]Department of Immunology, Genetics and Pathology, Uppsala University, 751 85 Uppsala, Sweden

[3] Department of Pharmacology, Oita University, Faculty of Medicine, Oita, Japan

[4]Department of Medical Cell Biology, Uppsala University, 751 23 Uppsala, Sweden

*** Corresponding authors:** Ingvar Ferby, e-mail:ingvar.ferby@igp.uu.se

Dorival Mendes Rodrigues-junior, dorival.mrj@imbim.uu.se

[#]These authors contributed equally

Running title: ErbB3 component of the endocytic machinery

Final character count (main text): 9072

ABSTRACT

Receptor tyrosine kinases (RTKs) are important cargo of endocytic trafficking, yet the role of RTKs in endocytic sorting and maturation of multivesicular bodies (MVBs) per se remains unclear. Here we show that the ErbB3 receptor, frequently overexpressed in invasive breast cancers, sorts internalized transferrin receptor (TfR) and Integrin β1 for endocytic recycling, in a manner that does not require ligand-induced ErbB3 signaling in breast epithelial cells. Loss of ErbB3 abrogates recycling of Integrin β1, likely from a Rab4-positive compartment, and redirects it towards lysosomal degradation or secretion as cargo of extracellular vesicles (EVs). Depletion of ErbB3 impairs migration of sheets of breast epithelial cells, concomitant with imposing a reduction of Integrin β1 cell surface level and an increase in release of EVs containing Integrin β1. In contrast, EVs secreted from ErbB3-depleted cells enhanced the motility of wild-type cells, potentially counteracting the reduced migration of ErbB3-deficient cells. Mechanistically, ErbB3 facilitates assembly of the Arf6-GGA3-Rabaptin5 endosomal sorting complex to promote early recycling, which consequently suppresses EV release. Therefore, ErbB3 constitutes part of the endosomal trafficking machinery, provoking the notion that RTKs might play a novel and yet unrecognised role in vesicular trafficking.

INTRODUCTION

The epidermal growth factor receptor (EGFR) family of receptor tyrosine kinases (RTKs), including EGFR, ErbB2, ErbB3 and ErbB4, form homo- or heterodimers and play key roles in epithelial development and homeostasis while their deregulation contributes to most epithelial cancers[1]. RTK dimers are activated upon ligand-binding, leading to recruitment of molecules that initiate intracellular signaling cascades. ErbB3 has limited kinase activity, but signals as heterodimers with other members of the EGFR family, and accumulating evidence highlights its potent oncogenic activity. In particular, ErbB3 has been linked to the migratory behaviour and metastasis of cancer cells and is responsible for acquired resistance to anti-EGFR therapies[2–6] .

Ligand-binding to RTKs also triggers receptor internalisation and trafficking within the cells which determines strength, duration and spatial distribution of EGFR signals[7–11]. RTKs, including EGFRs are internalised through clathrin-dependent and -independent mechanisms, converging on the delivery of the receptors to early endosomes[10]. Notably, although the mechanisms regulating ErbB3 turnover are still not fully understood, protein kinase C (PKC) has been linked promoting ErbB3 endosomal sorting[12]. Thereafter, RTKs are diverted towards either (i) back to the plasma membrane via recycling; (ii) protein degradation through lysosomes; or (iii) secretion in the extracellular milieu as cargo of small extracellular vesicles (EVs)[13,14]. The collective term EVs refer to a variety of secreted nanovesicles confined by a lipid bilayer, such as (i) exosomes which have endosomal origin and are formed upon the maturation of MVBs and released into the extracellular milieu or (ii) microvesicles originating from the plasma membrane, both mediating intercellular communication from secreting to recipient cells by carrying bioactive molecules [14,15].

Rab GTPases Rab4 ("short-loop") and Rab11 ("long-loop") are major regulators driving endosomal trafficking and recycling of RTKs and other transmembrane proteins, including Integrins[16–18]. Of note, the ubiquitously expressed GGA1-3 proteins, which are clathrin adaptors dependent on small GTPases of the Arf family, have been found to regulate Rab4 or

-11-dependent endosomal recycling of Integrin β1 (GGA2, GGA3), Transferrin receptor (TfR) (GGA1), Met RTK and Ret RTK (GGA3)[19–25]. GGA proteins contain several functional domains that bind to accessory proteins modulating membrane trafficking, including Rabaptin5[22,26–29], which promotes cooperatively a linker among Rab5- and Rab4-containing microdomains on early endosomes to coordinate the coupling of these domains[30], thereby regulating sorting of cargo including Integrin β3 and TfR into recycling endosomes[30–33].

We found a novel role for ErbB3 in vesicular sorting whereby it stabilizes the Arf6-GGA3-Rabaptin5 endosomal sorting complex, to promote early recycling of TfR and Integrin β1. Depletion of ErbB3 or its effectors Rabaptin5 or GGA3 re-routes Integrin β1 from endocytic recycling towards lysosomal degradation and secretion as EV cargo. Altogether, these findings depict a novel mechanism by which an RTK regulates endosomal events with potential impact on endocytic pathway-related biomedicine.

RESULTS

ErbB3 promotes endocytic recycling of transferrin receptor and Integrin β1

ErbB3 is highly expressed in breast cancer (BRCA) patients in comparison to healthy controls (extracted from TCGA datasets; Supplementary Fig S1A), which correlates significantly with a poorer overall survival of BRCA patients (Supplementary Fig S1B). Moreover, higher mRNA levels of *ErbB3* were associated with the lack of response of BRCA patients to chemotherapies (Supplementary Fig S1C), which is consistent with the known pro-tumorigenic role of ErbB3 in BRCA[2–6]. ErbB3 has been found to continuously endocytose and recycle back to the plasma membrane[13,34] in a manner that does not require ligand stimulation or other members of the EGFR family[13]. Thus, we wondered if endosomal trafficking of ErbB3 might be coordinated with, or even regulate endocytic trafficking and sorting of cargo that are recycled back to the plasma membrane, such as the transferrin receptor (TfR) that has been extensively studied as a cell surface receptor that undergoes internalisation and recycling with negligible sorting to

late endosomes and lysosomes[35]. TfR on the cell-surface of breast epithelial cells (MCF7) transfected with siControl (siCtrl) or siErbB3 were tagged with Alexa594-conjugated transferrin on ice for 30 minutes. Unbound labelled transferrin was washed away and cells incubated at 37°C in the presence of unlabelled transferrin for up to 1 hour. Cells were brought back on ice and subjected to low pH treatment to quench Alexa594 that had returned to the cell surface, followed by visualisation of chased transferrin retained in endosomes by fluorescence imaging (Figure 1A). After one h at 37°C, most TfR was recycled back to the plasma membrane as indicated by the shedding of labelled transferrin from the cells. However, half of the chased transferrin was still retained in endosomes in cells transfected with siErbB3 (Figures 1B and 1C).

Integrins are pivotal molecules regulating cell-cell adhesion and cell-extracellular matrix (ECM) interactions and the β1 subunit is the most common among the 18 α and 8 β subunits, forming the basis for cell survival and motility[36,37]. Since Integrin β1 is continuously internalised and recycled back to the plasma membrane, we wondered whether ErbB3 could colocalize with internalised Integrin β1 on MCF7 cells that express high levels of endogenous ErbB3, detectable by immunofluorescence. Briefly, Integrin β1 was labelled on ice with an Alexa488-conjugated antibody, and allowed to internalise for 15 minutes at 37°C, prior to fixation and immunolabeling of endogenous ErbB3. Confocal microscopy showed that ErbB3 and traced Integrin β1 colocalized on intracellular structures likely to be endosomes based on their estimated size (0.5-2 µm), as well as in filopodia (Figures 1D-1F). The degree of colocalization on putative endosomes was determined from deconvoluted confocal images by measuring enrichment of Integrin β1 on ErbB3-positive putative endosomes, relative to their adjacent surrounding cytoplasm (Figure 1G). Of importance, 32% of the ErbB3-positive endosomal structures showed prominent Integrin β1 enrichment (>100%) (Figure 1G).

We next investigated the putative role of ErbB3 in endocytic trafficking of Integrin β1 by conducting a recycling assay as outlined in Figure 1H. Briefly, the cell-surface pools of Integrin β1 were labelled with Alexa488-conjugated antibody on ice, prior to 15 minutes incubation at

37°C, time during which the internalised Integrins accumulate primarily in early endosomes[38]. The proportion of surface-labelling Integrin antibody that remained on the cell surface was then quenched with an anti-Alexa488 antibody on ice, as previously described[19]. Cells were subsequently incubated at 37°C and re-emergence of internalized Integrin β1 at the basal membrane was followed by live cell TIRF microscopy imaging (Figure 1H). In the non-malignant human breast epithelial cell-line MCF10A, about 70% of the chased Integrin β1 was detected at the plasma membrane already after 10 minutes (Figures 1I and 1J) and ErbB3 silencing, using two independent and validated siRNAs reduced recycling of Integrin β1 by 40-50% (Figures 1I and 1J; Supplementary Figure S2A). Similar results were obtained on primary non-malignant human breast epithelial cells prHMEC (Figures 1K and 1L; Supplementary Figure S2B), while Integrin β1 appeared to remain internalized for extended times in MCF7 cells both in siCtrl and siErbB3 transfected cells (data not shown). The initial amount of fluorophore-labelled Integrin β1 detected on the cell surface, prior to tracing, was 18-19% lower upon knockdown of ErbB3 compared with control in MCF10A (Supplementary Figures S2C and S2D) but unchanged in prHMECs (Supplementary Figures S2E, S2F) as determined by confocal imaging. No significant change in Integrin β1 levels was observed upon ErbB3 depletion in MCF10A (Supplementary Figure S3A) and prHMEC cells (Supplementary Figure S3B, S3C).

ErbB3 is a kinase-inactive receptor and it is known to act in a dimer with other members of the ErbB family. In order to determine whether either EGFR or ErbB2 plays a similar role to ErbB3 in endocytic recycling of Integrin β1, we subjected MCF10A cells to RNAi-mediated depletion of EGFR or ErbB2 prior to assaying endocytic recycling of Integrin β1 (Supplementary Figure S3A). Depletion of EGFR or ErbB2 did not impair Integrin β1 recycling (Figures 1M and 1N; Supplementary Figure S4A-E), suggesting that ErbB3 acts independently of its canonical heterodimer partners to promote endocytic recycling of Integrin β1. Of note, ectopic expression of siRNA-resistant ErbB3 restored the surface pool of traced surface-labelled Integrin β1 in ErbB3-depleted MCF10A cells, as visualized by confocal imaging (Supplementary Figures

S5A and S5B), indicating that off-target effects of the ErbB3 siRNAs do not underlie the observed recycling defect. ErbB4 was excluded from these experiments due to the lack of its expression in these cells, as previously reported[39,40].

Of importance, the recycling assays (Figure 1; Supplementary Figures, S2, S4 and S5) were conducted in a cell culture medium devoid of growth factors. Under these conditions we did not detect tyrosine phosphorylation of immunoprecipitated ErbB3 by immunoblotting with an antibody that recognises global phosphotyrosine (Supplementary Figure S5C), nor did we detect phosphorylation of ErbB3 on Tyr1289, or significant activation of the AKT and ERK1/2 kinases, typically observed downstream of ligand-stimulated ErbB3 (Supplementary Figure S3A). These results indicate that ErbB3 promotes TfR and Integrin β1 recycling in a manner that does not require ligand-induced receptor signaling.

ErbB3 guides Integrin β1 to the leading edge of motile epithelial cell sheets

Endocytic recycling is important for the polarised distribution of Integrins distribution in migrating cells[39–42]. In this context, Integrin β1 localizes to the leading edge of migrating epithelial cells in a Rab4-dependent manner[19,23]. To evaluate whether ErbB3 regulates the distribution of recycled Integrin β1 in sheets of migrating breast epithelia, a scratch was inflicted on confluent monolayers of MCF10A cells and incubated with surface labelling Alexa488-conjugated Integrin β1 antibody for 1 hour on ice, prior to removal of the antibody and subsequent incubation at 37°C for 1 hour (Figure 2A). Chased Integrin β1 and F-actin were visualized in cells at the leading front of the closing cell-sheets by immunofluorescence imaging (Figure 2B). Integrin β1 enrichment at the leading edge, or along cell-cell contacts relative to adjacent cytoplasm was quantified in cells bordering the scratch (boxed regions in Figure 2B). RNAi-mediated depletion of ErbB3 led to a 59.6% decrease in Integrin β1 enrichment at that leading edge, as compared with control siRNA treated cells after 1 hour of tracing at 37°C ($p=0.0016$) (Figure 2C). At cell-cell contacts, Integrin β1 enrichment decreases by 42.5%

($p<0.0001$) (Figure 2D). These results are consistent with a role of ErbB3 in recycling Integrin β1 to the leading edge of migrating cells and to a lesser extent to cell-cell contacts.

Given that endocytic recycling of Integrin β1 is important for cell motility, one would predict that loss of ErbB3 impairs cell migration. Remarkably, siRNA-depletion of ErbB3 reduced the rate of scratch closure in MCF10A cells compared to control (Figures 2E and 2F), with area under curve (AUC) increasing with 50.2% and 48.2% in mock vs. lapatinib-treated samples respectively (Figure 2G). Of note, this assay was performed in EGF-deprived but serum-containing media in the presence or absence of the dual EGFR/ErbB2 specificity inhibitor lapatinib, to eliminate influence of EGF-induced cell migration[43,44]. It is evident that under both conditions (mock and lapatinib) cell migration was not dependent on EGFR/ErbB2 signaling (Figure 2G). Cell proliferation, determined by EdU incorporation, did not differ between control or ErbB3 siRNA-transfected cells (Figure 2H), thus, in the absence of any impaired proliferation, the latter cannot contribute to the observed migration defect caused by loss of ErbB3. In summary, our data show that ErbB3 promotes migration of epithelial sheets in a manner that does not require canonical transphosphorylation of ErbB3 by EGFR or ErbB2.

ErbB3 colocalizes with Rab4-positive recycling endosomes and impairs extracellular vesicle release

It has been shown that TfR recycles via both Rab4- and Rab11-positive compartments[35,45]. Accordingly, our data shows a marked reduction in TfR and Integrin β1 recycling in ErbB3-depleted cells already 10 minutes post onset of tracing (Figure 1), which corresponds to the reported peak time when colocalization of Rab4 with traced TfR, preceding Rab11 and TfR colocalization that peaks later at 30 minutes[35]. To observe whether ErbB3 resides in recycling compartments, ErbB3-mCherry was co-expressed with either GFP-Rab4 or GFP-Rab11 in MCF10A cells, followed by treatment with either primaquine (PQ), an inhibitor of endocytic recycling[19,46], or vehicle alone for 10 minutes and subsequent visualisation of the proteins by

confocal imaging (Figure 3A). Colocalization was analyzed as enrichment of ErbB3 fluorescence in Rab4- or Rab11-positive compartments (Figure 3B) or visualized as average intensity projections of all structures (Figure 3C). Majority of ErbB3-mCherry did not colocalize with GFP-Rab4 or GFP-Rab11 positive structures in the absence of PQ-treatment. However, upon PQ-treatment for 10 minutes, ErbB3 enrichment in Rab4-positive structures increased 6.2-fold (p=0.0003), while no significant enrichment was observed in Rab11-positive structures (Figure 3B). The preferred ErbB3 colocalization with Rab4-positive rather than Rab11-positive recycling endosomes is consistent with ErbB3 having a role in promoting early Rab4-dependent recycling, although our data does not exclude its involvement in other Rab-dependent recycling routes. These data are in line with the observation that ErbB3 is required for early endocytic recycling already within 10 minutes (Figure 1), during which time the rapid Rab4-dependent recycling route is prominent[16,17].

We next addressed whether ErbB3 specifically regulates the recycling pathway or plays an additional role in exocytic trafficking. Thus, we used a well-established system to analyse exocytic trafficking from the endoplasmic reticulum (ER) using ectopically expressed vesicular stomatitis virus, VSV-G-ts-GFP[47]. The temperature sensitive form of VSV-G accumulates in the ER at 40°C and upon shift to 32°C, this protein traffics via the trans-Golgi-network (TGN) to the cell surface (Figure 3D). Of note, ErbB3 silencing in MCF7 cells did not affect the amount of VSV-G that was transported from the ER to the cell surface after 30 minutes, 1 or 2 hours at permissive temperature as monitored by immunoblotting of isolated surface-biotinylated proteins (Figures 3E and 3F and Supplementary Figure S6A, respectively). Immunoblotting against the transmembrane protein Muc1 on the isolated biotinylated proteins control for equal sampling. To complement the surface-biotinylation assay, traced VSV-G-ts-GFP was visualized by confocal imaging. In both siCtrl or siErbB3 transfected MCF7 cells, VSV-G-ts-GFP exhibited predominant localization in the ER at 40°C. Following shift to 32°C, VSV-G-ts-GFP was first detected in GM130+ TGN at 30 minutes and E-cadherin+ membrane compartment at 1 hour in both control and ErbB3 siRNA transfected cells (Supplementary

Figure S6B), suggesting that ErbB3 does not impact trafficking from the TGN to the plasma membrane.

Notably, a role for Rab4 in limiting exosome biogenesis by enhancing early endosomal recycling has been proposed[48]. To address whether impaired endocytic recycling caused by loss of ErbB3 could also influence EV release, we isolated small EVs secreted from MCF10A cells transfected or not with ErbB3 or non-targeting siRNAs (Figure 3G) by an established protocol of tangential flow filtration, followed by immune-affinity to the tetraspanin CD81, or by ultracentrifugation (UC) (Figure 3H)[49,50]. EVs enriched in the vesicular secretome fraction (VSF) were visualized by transmission electron microscopy (TEM), validating the presence of membrane-surrounded nanoparticles of 75–200 nm in size consistent with small EVs (Supplementary Fig S7A). Nanoparticle tracking analysis (NTA) revealed that the number of secreted EVs increased significantly in two independent ErbB3 silenced cells in comparison to siCtrl or to wild-type non-transfected cells, while the EV modal size was not affected (Figure 3I, Supplementary Figure S7B). Additionally, at equal sample volume, the expression of established EV markers, including the endosomal sorting complexes required for transport (ESCRT)-associated molecules ALIX and TSG101 or the tetraspanins CD81 and CD63 were increased in the same volume of EV fractions enriched by VSF, CD81-EVs or UC EVs from ErbB3-depleted cells (Figure 3J and 3K; Supplementary Figure S7C, respectively), validating the NTA results. Similarly, ErbB3 loss in prHMEC cells (Supplementary Figure S5D) did not impact the modal size of EVs, but significantly enhanced the EV release (Supplementary Figure S5E). Furthermore, RAB4A silencing in MCF10A cells (Figure 3L) significantly increased EV secretion (Figure 3M), which is in line with the previous findings of Zhang et al.[48]. Collectively, our data reveal a novel role for ErbB3 in promoting early endocytic recycling of different cell surface-derived receptors, and restricting EV secretion in non-tumorigenic breast epithelial cells.

ErbB3 loss directs Integrin β1 for lysosomal degradation and secretion in extracellular vesicles

We sought to trace the fate of internalised Integrin β1 that fails to recycle back to the cell surface in the absence of ErbB3. Towards this end, MCF10A cells were labelled with an Alexa488-conjugated surface binding Integrin β1 antibody on ice, followed by incubation at 37°C for 15 minutes to allow Integrin β1 internalisation and subsequent quenching on ice of the Integrin β1 that remained on the cell surface. Finally, the cells were returned to 37°C and the fate of the internalised pool of Integrin β1 was visualized by confocal fluorescence microscopy for up to half an hour (Figures 4A and 4B). Already after 15 minutes of tracing, Integrin β1 levels decreased by 42.4% in ErbB3-depleted cells at which time no significant change was observed in cells transfected with siCtrl (Figures 4B and 4C). Notably, Integrin β1 levels were somewhat reduced already at the onset of the tracing (0 h time point) in ErbB3-depleted cells compared to control cells (13.3%) (Figure 4C), which is probably due to accelerated Integrin β1 turnover in ErbB3 depleted cells evident within the 15 minutes internalisation step that precedes quenching and the onset of tracing (0 minute).

To assess the impact of ErbB3 on Integrin β1 turnover over an extended time period (up to 8 hours), we subjected control or ErbB3 siRNA-transfected MCF10A cells to treatment with the protein synthesis inhibitor cycloheximide (CHX) and monitored Integrin β1 levels by immunoblotting (Supplementary Figures S8A and S8B). While Integrin β1 levels were slightly reduced for up to 8 hours in the presence of CHX in the control cells, their levels were significantly decreased by 72% after 8 hours of CHX treatment in ErbB3-depleted cells (Supplementary Figures S8A and S8B). To evaluate directly Integrin β1 stability, we performed a pulse-chase analysis of Integrin β1 turnover. Control or ErbB3 siRNA-transfected MCF10A cells were labelled with ^{35}S-methionine/cysteine for 1 hour, followed by chasing with un-labelled amino acids at 37°C. Integrin β1 was subsequently immunoprecipitated and the protein incorporated ^{35}S-label was determined by radiography. The data show that cells

transfected with two independent siRNAs against ErbB3 exhibited a significantly accelerated Integrin β1 turnover (49% or 84% decrease), compared to control cells (Figures 4D and 4E).

The turnover of Integrin β1 is slow, yet, limited degradation of this protein has been found to occur in the lysosomes[51]. To better characterize Integrin β1 turnover, we traced surface-labelled Integrin β1 in control or ErbB3 siRNA transfected MCF10A cells by confocal fluorescence microscopy, in the presence or absence of chloroquine, which impairs phagolysosomal fusion (Figure 4F). Chloroquine treatment caused traced Integrin β1 to accumulate in cells bordering the migratory front of scratched monolayers of both wild type and ErbB3-depleted cells (Figures 4G). Quantification of fluorescence intensity showed that while the level of traced Integrin β1 was reduced in the ErbB3-depleted cells relative to siCtrl cells (by 44.8%, $p<0.0001$), consistent with its increased turnover, chloroquine treatment significantly restored traced Integrin β1 levels (Figure 4H). Our results indicate that elevated Integrin β1 turnover caused by ErbB3-loss is in part due to increased lysosomal degradation.

It has been reported that EV-associated Integrins assist organotropic metastasis[52] and in particular Integrin β1 found to be associated with increased tumor invasiveness and metastatic potential of BRCA cells[36]. In this context, we sought to assess whether the sorting of Integrin β1 into EVs could be affected by ErbB3 silencing. We found that siRNA-mediated depletion of ErbB3 (Figure 4I) increased the amount of UC EV-associated Integrin β1, as detected by immunoblotting (Figure 4J). The prevalence of EVs in the UC samples were further validated by the increased presence of ALIX and TSG101, in addition to the absence of the Golgi marker GM130 (Figure 4J), and membranous nanovesicles labelled with CD63-immuno-gold were visualized by TEM (Figure 4K), attesting to the EV integrity. These results imply that the increased turnover of Integrin β1 in ErbB3-silenced cells occurs both through lysosomal degradation and through EV secretion.

We hypothesised that EVs carrying Integrin β1 could be involved in promoting invasive properties or viability of the breast epithelial cells. We therefore stimulated MCF10A cells with normalized concentrations of VSF (1×10^9 nanoparticles/mL) derived from either siCtrl or

siErbB3 treated cells for 48 hours and assessed cell viability by PrestoBlue fluorescence or invasion into ECM (Matrigel). We found that EVs from both control or ErbB3-depleted cells promoted cell viability to the same extent (Figure 4L), while EVs derived from ErbB3-depleted, but not control cells, enhanced motility of MCF10A cells into a Matrigel matrix (Figure 4M). Together, our results indicate that while ErbB3-silenced MCF10A cells exhibited lower motility in the scratch assay (Figure 2), they can elevate invasive behaviour of neighbouring wild-type cells by releasing a larger amount of Integrin β1-containing EVs with enhanced motility promoting properties.

ErbB3 promotes assembly of the Arf6-Rabaptin5-GGA3 sorting complex and stability of Rabaptin5 and GGA3

We explored mechanistically whether ErbB3 interacts with selected components of the endosomal machinery that could be implicated in the Rab4-dependent early recycling of Integrin β1. Towards this end, we immunoprecipitated endogenous ErbB3 from MCF10A cell extracts and examined co-precipitates by immunoblotting against the ADP-ribosylation factor-binding protein GGA3 (GGA3), which was previously reported to be required for Rab4-dependent recycling of Integrin β1[19] and the Rab GTPase-binding effector protein 1 (Rabaptin5 or RABPT5), which is an accessory protein to the GGA family[26] and has been shown to regulate Rab4-dependent recycling of Integrin β3[31]. Interestingly, we found that ErbB3 co-precipitated efficiently with both GGA3 and Rabaptin5 at endogenous levels (Figure 5A) and the abundance of this complex was increased after a 30-minute treatment with PQ, consistent with these proteins interacting in the recycling compartment. Thus, GGA3 and Rabaptin5 are plausible effectors of ErbB3 in the trafficking control of early endosomes.

GGA3 has been shown to interact with ADP-ribosylation factor 6 (Arf6) to drive recycling of different transmembrane proteins[23,53] and with Rabaptin5 to regulate TGN cargo export and endosomal tethering/fusion events[26,27]. We therefore set out to determine the influence of

ErbB3 on the Arf6-GGA3-Rabaptin5 network formation (Supplementary Figure S9A). Thus, MCF10A cells were transfected with control or ErbB3 siRNA, prior to treatment with PQ or vehicle alone for 10 minutes. Harvested cell lysates were subsequently subjected to Arf6 immunoprecipitation and immunoblotting for bound GGA3 and Rabaptin5 (Figure 5B). The data revealed that loss of ErbB3 indeed reduced the amount of GGA3 and Rabaptin5 associated with Arf6 both in the absence and in particular in the presence of PQ, which interestingly, led to a stronger interaction of ErbB3 with GGA3 and Rabaptin5 (Figure 5A). Of note, Rabaptin5 and GGA3 protein levels were reduced in ErbB3-depleted cells (Figure 5C), which could explain the reduced interaction. Nevertheless, the lower protein levels of GGA3 and Rabaptin5 was not due to their reduced transcription, as determined by RT-qPCR (Figure 5D), suggesting reduced protein stability. This data is supported by the observation that treatment of ErbB3-depleted MCF10A cells with the proteasome-inhibitor MG132 partially restored GGA3 and Rabaptin5 protein levels (Supplementary Figure S9B). It is possible that reduced engagement of GGA3 and Rabaptin5 in a stable complex with ErbB3, underlies its proteasomal degradation.

Interestingly, we noted that ErbB3 has a unique putative GGA3-binding motif (DxxLL) in the activation loop of the pseudokinase domain, that is not found on EGFR or ErbB2 (Figure 5E). The DxxLL motif constitutes a consensus binding site for VHS domains found in GGA proteins. To test whether ErbB3 binds GGA3 via this motif, we mutated the two conserved leucines in ErbB3 to alanine (LL866/7AA). GGA3 was overexpressed with or without ErbB3 wildtype or the LL866/7AA mutant in HEK293T cells followed by immunoprecipitation of ErbB3 and immunoblotting against GGA3 (Figure 5F). We found that GGA3 co-immunoprecipitated with wild-type but not the LL866/7AA mutant ErbB3 (Figure 5F), suggesting that ErbB3 interacts with the VHS domain of GGA3 (Figure 5E). Thus, we tested the hypothesis that ErbB3 scaffolds the assembly of the Arf6-GGA3-Rabaptin5 complex by ectopically expressing these proteins in HEK293T cells with or without wild-type or LL866/7AA mutant ErbB3, followed by immunoprecipitation of Arf6 and immunoblotting analysis of associated ErbB3, GGA3 and

Rabaptin5. We found that GGA3 and Rabaptin5 co-precipitated more efficiently with Arf6 in the presence of wild-type but not mutant ErbB3(LL866/7AA) (Figure 5G). Furthermore, apart from interacting with GGA3, and in line with a scaffolding function for ErbB3, we found that ErbB3 directly binds Rabaptin5 in vitro, in pull-down experiments of recombinant GST-ErbB3 incubated with recombinant MBP-Rabaptin5 (Supplementary Figure S7C). Taken together, our data suggest that ErbB3 acts as a scaffold that associates with both GGA3 and Rabaptin5 to promote the assembly of the Arf6-GGA3-Rabaptin5 endosomal sorting complex. In the absence of ErbB3, GGA3 and Rabaptin5 protein levels are reduced possibly as a consequence of their release from this sorting complex.

Rabaptin5 and GGA3 are effectors of ErbB3 in endosomal trafficking

Previous studies reveal critical importance of Rabaptin5 for directing Integrin β3 towards Rab4-dependent recycling[31,54], however the same has not yet been demonstrated for Integrin β1. Thus, we traced surface-labelled Integrin β1 in MCF10A cells transfected with either control or Rabaptin5 siRNA and visualized the re-emergence of internalized Integrin β1 at the basal membrane by TIRF live cell imaging (Figure 6A). Depletion of Rabaptin5 caused a significant reduction in the rate and amount of Integrin β1 that recycled back to the basal membrane (Figures 6B and 6C), quantified as a significant decrease of 28.7% in AUC.

Furthermore, we examined the impact of Rabaptin5-depletion on Integrin β1 stability by pulse-chase analysis of protein turnover. Control or Rabaptin5 siRNA-transfected MCF10A cells were labelled with ^{35}S-methionine/cysteine for 1 hour, followed by chasing with un-labelled amino acids at 37ºC. Integrin β1 was subsequently immunoprecipitated and the incorporated ^{35}S-label was determined by autoradiography. The data shows that Rabaptin5-depleted cells exhibited accelerated Integrin β1 turnover, with a significant 49% reduction in 9 hours when compared to control-treated cells (Figures 6D and 6E). Likewise, previous work has shown

that siRNA-mediated silencing of GGA3 re-routes Integrin β1 from Rab4-dependent recycling towards lysosomal degradation[23].

We next assessed the impact of Rabaptin5 or GGA3 on EV release from MCF10A cells. Thus, NTA revealed a significant increase of small EVs release upon Rabaptin5 knockdown, without impairing the EVs' modal size (Figure 6F), while TEM confirmed the presence of membrane-surrounded nanovesicles in the enriched VSF (Figure 6G). Moreover, MCF10A cells transfected with siCtrl, siErbB3 or siGGA3 (Figure 6H) had their EVs enriched by UC and characterized by NTA, indicating that GGA3 depletion enhanced significantly EV release in comparison to the siCtrl cells (Figure 6I), similar to ErbB3-depletion (Figure 3). In line with this finding, further analysis of different positive and negative EV markers by immunoblotting showed enrichment of ALIX, TSG101 and Integrin β1 in the UC EV fraction upon ErbB3 or GGA3 depletion, while the Golgi marker GM130 was absent (Figure 6J). Of note, the morphology of these EVs was observed by TEM (Figure 6K). Hence, loss of either GGA3 or Rabaptin5 mimics the effect of loss of ErbB3 on endocytic trafficking of Integrin β1, consistent with the hypothesis that GGA3 and Rabaptin5 are effectors of ErbB3 in promoting endosomal recycling and impeding EV release.

DISCUSSION

We report that the RTK family protein ErbB3 promotes endocytic recycling of TfR and Integrin β1 in a ligand-independent manner, as well as that ErbB3 restricts the release of EV-associated Integrin β1. Endocytic trafficking of RTKs provides critical spatial and temporal control of the intracellular signaling events they trigger, which ultimately governs cellular response. Hence, the mechanisms by which RTKs internalise and traffic within the cell has been subject to intense scrutiny. While prevailing knowledge centres on RTKs as vesicular passengers, our study provides a compelling example of an RTK family member playing an integral role in the endocytic trafficking machinery per se.

RTK signaling is integrated at many levels with the regulation of endocytic trafficking of Integrins[46,55,56]. Growth factor mediated activation of AKT or protein kinase D (PKD) can for example regulate Integrin recycling by phosphorylating proteins, such as ACAP1, an ARF6GAP[57], or Rabaptin5[31], respectively. Conversely, several studies have shown that Integrins alter recycling of other receptors, such as EGFR[58] and vascular endothelial growth factor receptor (VEGFR2)[59], further highlighting the close coordination of Integrins and with RTK trafficking. We found that ErbB3 can promote endocytic recycling of TfR and Integrin β1, independently of canonical ErbB3-driven tyrosine kinase signaling. Intriguingly, EGFR has been reported to function in a ligand-independent manner to scaffold an exocyst subcomplex needed to assemble autophagosomes[60]. This invites wider speculation that 'inactive' RTKs, as exemplified by EGFR and ErbB3, might play an instrumental role in intracellular vesicular trafficking as scaffolding centres.

We show that ErbB3 interacts with both GGA3 (via its VHS domain) and Rabaptin5 to promote assembly and stability of the Arf6-GGA3-Rabaptin5 endosomal sorting complex. GGA3 has previously been reported to be required to sort multiple cargos, such as Integrin β1, c-Met and c-Ret for Rab4-dependent recycling[20,21,23]. It is therefore possible that ErbB3 drives recycling of not only TfR and Integrin β1 as reported here, but all cargo that depends on Arf6-GGA3, although this remains to be addressed. Furthermore, loss of ErbB3 redirects Integrin β1 towards lysosomes for degradation, mimicking loss of GGA3 that similarly redirects both Integrin β1[23] and c-Met towards lysosomal degradation[21], or Rabaptin5 depletion that we find similarly redirects trafficking of internalised Integrin β1 towards lysosomal degradation. Taken together these results lead us to propose that ErbB3 engages into endocytic recycling by promoting formation and stability of the Arf6-GGA3-Rabaptin5 vesicular adaptor complex, in line with the emerging concept that pseudo-kinases have evolved to acquire scaffolding functions. In addition to this, it has been shown by others that Arf6 interacts with Phospholipase D2, to promote synthesis of phosphatidic acid and thereby formation of syntenin-ALIX intraluminal vesicles, which are later secreted as exosomes[61]. Likewise, ARF6 activation leads

to the phosphorylation of myosin light chain (MLC) and actomyosin contraction, which allows the vesicles to bud off from the membranes of cancer cells[62]. Thus, since ErbB3 promotes the assembly of the Arf6-GGA3-Rabaptin5 complex, we speculate that ErbB3 association with GGA3 could negatively control EV release by retaining Arf6 at early endosomes, which could suppress the formation of Arf6-PLD2-PA complexes, explaining the reduced EVs secretion in breast epithelial cells, although further studies are required to address this hypothesis.

Activation of EGFR and ErbB2 involve formation of asymmetric kinase domain dimers, whereby one kinase domain acts as an 'activator' and the other as a 'receiver', that becomes activated[63,64]. However, the ErbB3 pseudo-kinase domain acts only as an activator while the receiver interface diverges in sequence from other ErbB receptor family members and is not engaged in kinase domain dimerization[63]. Interestingly, GGA3 interacts with a DxxLL motif situated on the activation loop within the dysfunctional catalytic site in the ErbB3 pseudokinase domain. This motif is not present in other ErbB receptor family members, where the corresponding position is instead involved in regulating kinase activity. It is tempting to speculate that the dysfunctional catalytic domain in ErbB3 may have evolved a novel kinase-independent function in regulating endocytic trafficking, perhaps shedding some light on the enigmatic nature of pseudokinases.

Previous studies have found that Integrin β1 can physically interact with EGFR and endocytose together[58,65]. Although ErbB3 and Integrin β1 were partly co-localised at focal adhesions and cell-cell contacts, we did not find that ErbB3 depletion influenced Integrin β1 internalisation. Thus, it remains to be elucidated whether ErbB3 and Integrin β1 associate during endocytosis. Notwithstanding, our results suggest that ErbB3 encounters Integrin β1 in sorting endosomes, presumably at the step when the cargo is sorted into Rab4-positive vesicles through engagement of the Arf6-GGA3-Rabaptin5-complex. This is suggested by the observation that Integrin β1 and ErbB3 colocalization was primarily observed upon treatment with the recycling inhibitor primaquine, when ErbB3 is retained in a Rab4-positive compartment, which coincides with enhanced binding of ErbB3 to GGA3 and Rabaptin5. This is in accordance with previous

work showing that GGA3 is enriched in Rab4-positive endosomes along with endocytosed Met, and to a much lesser extent Rab5-positive early endosomes[53].

The proposed role of ErbB3 in sorting of TfR, Integrin β1 and possibly other cargo into recycling endosomes, postulates that ErbB3 frequently resides in the sorting compartment independent of ligand-stimulation. In line with this prediction, ErbB3 has been found to continuously endocytose and recycle back to the plasma membrane[13,34,66] independent of both ligand stimulation and other members of the EGFR family[34]. Intriguingly, dynamic availability of ErbB3 in vesicular compartments may also be regulated independently of EGFR and ErbB2 since steady-state protein levels of ErbB3, but not EGFR or ErbB2, are tightly controlled by ligand-independent ubiquitination by the E3-ligase Nrdp1 that localizes in perinuclear membranes and targets ErbB3 for proteasomal degradation[67,68]. Furthermore, we found that ErbB3-dependent cell sheet migration also does not require EGF or other growth factors. It is however noteworthy to stress that growth factor-induced EGFR or ErbB2 signaling is well known to promote cell migration, and our data does not rule out or address the possible ErbB3 cooperation with EGFR or ErbB2 to drive growth factor-induced cell motility. In this manuscript, we focus entirely on the unexpected and growth factor-independent roles of ErbB3, distinguishing our investigation from the frequently studied and complex growth factor-induced cell signaling events.

Hence, our data points to ErbB3 regulating Integrin β1 delivery to the leading edge of migrating sheets of epithelial cells, promoting their migration. Since several studies established that Integrin recycling promotes cell migration and cancer cell invasiveness[58,69], we reveal a new perspective of how ErbB3 could mechanistically contribute to cell dissemination in part by promoting Integrin recycling. Conversely, we speculate that loss of ErbB3 could lead to increased dissemination of heterogeneous tumours by increasing release of integrin-containing EVs, with the potential to increase invasiveness of surrounding wild-type cells. Our study reveal that the pseudo-kinase ErbB3 plays a role in the vesicular sorting machinery by promoting rapid endosomal recycling of other cargo and impeding EV release. It invites the

wider speculation that other pseudo-RTKs may also have evolved scaffolding functions that might play instrumental roles in vesicular trafficking.

Acknowledgements

We thank Marino Zerial, Lukas Huber and Martin Offterdinger for kindly providing cDNA constructs. We also thank Carl-Henrik Heldin for valuable discussion and for critically reading the manuscript. This research was supported by the Swedish Cancer Society, grants CAN2018/469 and CAN2021/1506Pj01H (A.M.); the Swedish Research Council, grant 2018-02757 and 2023-02865 (A.M.), Lars Hierta Memorial Foundation, grant FO2023-0501 (D.M.R-Jr); O.E. och Edla Johanssons Vetenskapliga Stiftelsen (D.M.R-Jr); Stiftelsen Längmanska kulturfonden, grant BA24.0451 (D.M.R-Jr).

Author Contributions

D.M.R-Jr., A.R.S., T.T., O.I., T.M. and I.F. conceived and designed the experiments; D.M.R-Jr., A.R.S., J.S., O.I. and N.D. performed the experiments; D.M.R-Jr., A.R.S., O.I. N.D., A.M and I.F. interpreted the results; D.M.R-Jr., A.R.S. and I.F. wrote the manuscript, with input from all authors.

Declaration of Interests

The authors declare no competing interests.

Data and materials availability

Further information and requests for resources and reagents should be directed to and will be fulfilled by the Lead Contacts, Ingvar Ferby (ingvar.ferby@igp.uu.se) and Dorival Mendes Rodrigues-Junior (dorival.mrj@imbim.uu.se). The plasmids generated in this study are available upon request.

MATERIALS AND METHODS

Correlation analysis of gene expression

ErbB3 mRNA expression comparison in BRCA tumor versus normal samples was retrieved from the GEPIA2 server (https://gepia2.cancer-pku.cn/)[70]. BRCA patients overall survival was acquired using the KM plotter database (KMplot)[71]. Correlation of *ErbB3* mRNA expression and chemotherapy response in BRCA patients was conducted using the ROC Plotter database (http://www.rocplot.org)[72]. BRCA patients were categorized as non- or responders to treatment, according to the relapse-free survival status at five years post-surgery.

Cell lines and treatments

MCF10A cells were cultured in DMEM/F12 (Gibco) supplemented with glutamine (Sigma-Aldrich), 5% horse serum (Gibco), 20 ng/ml epidermal growth factor (EGF) (Miltenyi Biotech), 0.5 mg/ml hydrocortisone, 100 ng/ml cholera toxin and 10 µg/ml insulin (all from Sigma-Aldrich). Where indicated, a starvation medium lacking serum, insulin and EGF was used. Primary human mammary epithelial cells (prHMECs) from Gibco were cultured in HMEC ready medium (Invitrogen). MCF7 cells were cultured in EMEM supplemented with 0.01 mg/ml human recombinant insulin and 10% foetal bovine serum (FBS). HEK293T cells were cultured in DMEM (Sigma-Aldrich) with 10% FBS (Gibco). Unless otherwise stated, the cell lines were purchased from ATCC. Culture conditions were 5% CO2 at 37°C. For immunocytochemistry coverslips were coated with type I bovine collagen solution (Advanced BioMatrix) in 1:1000 in 0.02 M acetic acid overnight prior to application of cells.

The EGFR/ErbB2 inhibitor lapatinib was used at 1 µM (LC Laboratories) and was batch-tested for efficiency; cycloheximide at 50 µM (from Sigma-Aldrich); chloroquine at 50 µM (#14774 from Cell Signaling); primaquine (PQ) at 0.5 mM (#160393 from Sigma-Aldrich) for 10 or 30 minutes; MG132 (Calbiochem) at 50 µM. In all cases, control cells were treated with vehicle alone (DMSO, from Sigma-Aldrich) at the corresponding concentration.

Transfections

Cells were transfected with RNAiMAX (Invitrogen) according to the supplier's instructions. A final concentration of 20 nM of the following siRNAs were used: siErbB3#1 (5'CAAUACCAGACACUGUACAAGCUCU53'); siErbB3#2 (5'UCGUCAUGUUGAACUAUAA3'); siRab4A (5'GAACGAUUCAGGUCCGUGATT); siRabaptin5 (5'CCGGGCAAUUCUGAAUGAUACUAAA3'); siGGA3 (5'CCCGGGUCAUCAACUCUUATT3') or scramble siRNA (siCtrl: non-targeting pre-designed ID 12935112). All siRNAs were purchased from Invitrogen and the silencing experiments were performed 48 hours post transfection.

cDNAs and DNA transfection

MCF10A cells were transfected with Lipofectamine 3000 (Invitrogen) according to the supplier's instructions. Constructs for Rab4, Rab11 and Rabaptin5 were kindly provided from Marino Zerial (MPG Dresden, Germany), and mCherry- and Citrine-tagged ErbB3 were kindly provided by Martin Offterdinger (Innsbruck, Austria). Rabaptin5 was subcloned into pMALC2 for bacterial expression (see below). mCherry-tagged Rabaptin5 and YFP-tagged Arf6 were from Addgene. Flag-ErbB3 cDNA was subjected to site-directed mutagenesis (Agilent) to generate LL866/7AA mutant Flag-ErbB3. For rescue experiments mCherry-ErbB3 carrying two non-sense point mutations in the siRNA-recognition sequence was subcloned into pAdEasy XL and adenovirus produced using the AdEasy XL adenovirus system (Agilent) according to the manufacturer's instructions and MCF10A cells infected at a titter that yielded ErbB3 overexpression in approximately 90% of the cells.

RT-qPCR

RNA was extracted with the RNeasy Mini Kit (#74104 from Qiagen). cDNA was synthesized with the iScript™ cDNA Synthesis Kit (#170-8891 from Bio-Rad). qPCR was performed using the KAPA SYBR® Fast and primers for *ITGB1* (5'AGATCCGAAGTTTCAAGGGC3' and

5'GAACCATGACCTCGTTGTTC3'), *GGA3* (5'GGGACAGGGTGTCTGAGAAAG3' and 5'GTGCCTCGTCTTCCTTCACC3'), *RABEP1* (5'TTCCCAGCCTGACGTTTCTC3' and 5'GCTGCTGTTGTGCACGTAAA3') and *GAPDH* (5'CCCTTCATTGACCTCAACTA3' and 5'CCAAAGTTGTCATGGATGAC3'). The comparative Ct method was used to calculate fold change in gene expression relative to *GAPDH*.

Antibodies

The following primary antibodies were used: anti-ErbB3 (clone 2F12; Upstate Cell Signaling Solutions) for IP; anti-ErbB3 (clone D22C5; Cell Signaling) for immunoblotting; anti-Integrin β1 (monoclonal, ab52971 from Abcam, and clone TS2/16 from Biolegend for immuno-TEM). Moreover, anti-phospho-ErbB3 Tyr1289 (#4791, Cell Signaling Technology); anti-EGFR (#2232, Cell Signaling Technology); anti-ErbB2 (06-562, Millipore); anti-phospho-AKT Thr308 (#2965, Cell Signaling Technology); anti-AKT (#9272, Cell Signaling Technology); anti-phospho ERK1/2 (#9101, Cell Signaling Technology); anti-ERK1/2 (#9102. Cell Signaling Technology); anti-Total p-Tyr ab (4G10 platinum); anti-E-cadherin (#610182, BD Transduction Laboratories); anti-Muc1 (Cell Signaling Technology); anti-Alix (clone 1A12, SantaCruz Biotechnology); anti-CD81 (clone B11, SantaCruz Biotechnology); anti-CD63 (clone H5C6, Biolegend); anti-GM130 (clone 35, BD Biosciences); anti-Rabaptin5 (monoclonal, sc-271069 from SantaCruz Biotechnology); anti-GGA3 (clone 8; BD Transduction Laboratories); anti-Arf6 (clone 3A-1, SantaCruz Biotech.); anti-GAPDH (clone 14C10; Cell Signaling); anti-α-Tubulin (clone T5168, Sigma-Aldrich); anti-β-Actin (##sc-69879 SantaCruz Biotechnology); HRP-conjugated goat anti-mouse or goat anti-rabbit (The Jackson Laboratory) secondary antibodies were used for immunoblotting. Alexa fluor® 594 or Alexa fluor® 488-conjugated anti-rabbit antibodies (The Jackson Laboratory) were used for immunocytochemistry. For the Integrin recycling assay, Alexa Fluor® 488 anti-human Integrin β1 antibody (clone TS2/16, Biolegend) was used.

Immunoblotting and immunoprecipitation

Cells were lysed in sodium dodecyl sulphate (SDS)-sample buffer (120 mM Tris-HCl pH 6.8, 3 % SDS, 15 % glycerol, 0.03 % bromophenol blue, 75 mM dithiothreitol (DTT) and run on 8-10% polyacrylamide gels. Proteins were transferred onto Hybond™-P polyvinylidene fluoride (PVDF) membranes at 100 V for 120 minutes at 4°C. Membranes were blocked in 4% milk or 5% bovine serum albumin (BSA), dissolved in TTBS (tris-buffered saline, 0.1% Tween 20). The protein bands were visualized using ECL™ or ECL plus™ reagents and Hyperfilm® ECL (all from GE Healthcare) and detected with a CCD camera (Biorad). Quantification of western blots was performed using the ImageJ software.

For ErbB3 immunoprecipitation cells were lysed in: 1% NP40, 50mM Tris HCl pH8.0, 150mM NaCl, 0.5% sodium deoxycholate, 0.1% SDS and 1mM EDTA supplemented with Halt™ phosphatase/protease inhibitor (ThermoFisher Scientific). Preclearing of lysates was performed by incubating samples for 1 hour at 4°C under rotation with Pierce control agarose resin. Antibody incubation was performed overnight 4°C under rotation and precipitates washed 4 times in lysis buffers. Precipitated proteins were resolved by immunoblotting. Arf6 immunoprecipitations was performed as above but with lysis buffer: 1% Triton-X100, 100 mM sodium chloride (NaCl), 50mM Tris-HCl pH 7.4. Immuno-isolation/detection kits (coupled to CD63 or CD81 antibodies) were purchased from ThermoFisher Scientific and used after ultracentrifugation. The 100K pellets were re-suspended in 100µL PBS with 0.1% BSA (filtered through a 0.2 µm filter) and mixed with 100µL of magnetic beads slurry conjugated to the corresponding antibody according to the manufacturer's instructions.

Immunocytochemistry

MCF10A or MCF7 cells were cultured on collagen I-coated coverslips and fixed with 4% PFA in PBS for 20 minutes, permeabilized with 0.5% Triton in PBS for 10 minutes and then blocked in Superblock T20 blocking buffer (ThermoFisher Scientific). Primary and secondary antibodies and, where indicated, Alexa fluor® 488-conjugated Phalloidin (Life Technologies)

were diluted in blocking buffer. Coverslips were mounted using ProLong® Antifade Reagent (Life Technologies) with or without DAPI. Images were taken with a Leica SP8 (confocal) or Zeiss Axio Imager M2 (epifluorescence) microscopes and processed using Leica Suite or Zeiss ZEN 2011 software, respectively. Deconvolution of confocal image stacks was carried out in Huygens Essential 19.04 (Scientific Volume Imaging B.V.) using a theoretical PSF, automatic background estimation and CMLE deconvolution algorithm. The final signal to noise ratio was set to 10.

Transferrin recycling assay

MCF7 cells were incubated in starvation media supplemented with 25 mM HEPES for 3 hours prior to the assay. Cells were treated with 5 µg/mL of Alexa fluor®-conjugated transferrin (T13343, from ThermoFisher Scientific) for 30 minutes on ice. Thereafter, excess of labelled transferrin was removed by three washes with PBS and subsequently incubated in media containing 50 µg/ml unlabelled holo-transferrin (T4132, from Sigma-Aldrich) for the indicated times (0, 10, 30, 60 minutes). Finally, the cells were treated with an acidic solution (0.2 M acetic acid and 0.5 M NaCl) for 30 seconds to remove surface labelling, fixed in 4% PFA in PBS for 20 minutes at room temperature and mounted. Quantification performed on tree independent experiment. Mean cell intensity was measured with ImageJ (n>17 images of 1-4 cells for each data point). MCF7 cells were chosen for this assay due to efficient surface-labelling with Alexa fluor®-conjugated transferrin. Attempts to perform the transferrin-recycling assay in MCF10A cells were unsuccessful, due to insufficient surface-labelling with Alexa fluor®-conjugated transferrin in these cells.

Integrin recycling assay

MCF10A cells were plated on collagen-coated 24-well plates either sparsely or at high confluency for subsequent scratching. Cells were growth factor-deprived for 3 hours and then put on ice for 5 minutes to cool down. Surface Integrin β1 was labelled at 4°C during 45 minutes, then washed twice with PBS and returned to 37°C in order to allow internalisation.

After 15 minutes, cells were put back on ice and treated for 1 hour with anti-Alexa fluor® 488 (#A11094 from Life Technologies) in order to quench the remaining surface signal. After quenching, cells were again washed twice with PBS and incubated in deprivation media at 37°C. At indicated times cells were fixed with PFA 4% in PBS for 20 minutes at room temperature. When only Integrin internalisation was monitored, the quenching step was not performed. Quantification of total pixel intensity per cell, mean pixel intensity and average projections were performed with ImageJ.

TIRF microscopy

A prism-type TIRF microscope built around a Nikon E600FN upright microscope equipped with a 16× 0.8-NA water-immersion objective was used. The output from diode-pumped solid-state lasers (Cobolt, Stockholm, Sweden) were merged by dichroic mirrors and homogenized and expanded by a rotating, light-shaping diffusor (Physical Optics Corp., Torrance, CA). Excitation light was selected by interference filters (491 nm for Alexa-488 and 561 nm for mRFP, Chroma) mounted in a filter wheel (Lambda 10-3, Sutter Instruments, Novato, CA) and refocused through a modified dove prism (Axicon, Minsk, Belarus) at a 70° angle to achieve total internal reflection. Cells grown on 25-mm glass coverslips (Menzel-Gläser, #1) were kept on ice and mounted in a modified Sykes-Moore perfusion chamber just before imaging, placed on top of the prism and perfused with DMEM+F12 at a rate of 0.1 mL/minute. Emission wavelengths were selected with interference filters (525/25 nm for Alexa 488, 590/20 for mRFP, Chroma) mounter in a filter wheel (Sutter Instruments) and fluorescence was detected by a back-illuminated EM-CCD camera (DU-887, Andor Technology, Belfast, Northern Ireland). Filter wheels and camera were controlled by MetaFluor (Molecular Devices Corp., Downington, PA) and images were acquired every 10 seconds. An electronic shutter prevented light exposure between image captures. Imaging was done at 37°C.

TIRF microscopy images were analyzed off-line using ImageJ. Briefly, cell footprints were manually identified and regions of interest covering the edges of the adherent cells were drawn. Intensity changes within these regions through the time course of the experiment (45 minutes)

were measured and exported to Excel. All data points were background corrected, followed by normalization to the pre-stimulatory level (F/F0). Cells within large cell clusters were excluded from the analysis.

Wound healing assay

MCF10A cells were seeded in Falcon Multiwell 48-well plates and grown to full confluency. Before performing the wound, cells were pre-treated with 1 µM lapatinib or DMSO alone in serum-containing media lacking added growth factors for 1 hour. Thereafter, a scratch was placed in the middle of each well with a sterile pipette tip. After two washes with PBS, lapatinib/DMSO-containing growth-factor deprived but serum containing media was added back to the cells and the wound healing process was monitored using an IncuCyte ZOOM 40008 microscope for 14 hours. The obtained images were analyzed using the FIJI software.

^{35}S-Met/Cys pulse-chase protein turnover assay

MCF10A cells transfected with control or ErbB3 siRNA were incubated with growth factor deprived DMEM media lacking methionine and cysteine supplemented with 10 µCi/ml ^{35}S-methionine/cysteine (Perkin Elmer) for 30 minutes at 37°C. The labelling media was replaced with growth factor deprived MCF10A culture media containing 5 mM L-cysteine and 5 mM L-methionine (Sigma) for the indicated times, prior to cell lysis and immunoprecipitation of Integrin β1, SDS-polyacrylamide (PAGE) gel electrophoresis and detection of incorporated radioactivity using a Phosphoimager. Images were scanned and quantification of three independent experiments was perform in ImageJ.

Recombinant protein purification and *in vitro* binding assay

pMalC2-Rabaptin5 was transformed into the BL21S(DE3)pLysS bacterial strain (Invitrogen). Protein expression was induced with 0.3 mM IPTG for 2 hours at 37°C and recombinant MBP-rabaptin5 was purified with an amylose resin (New England Biolabs) according to the manufacturer's instructions and dialysed against lysis buffer (20 mM Tris-HCl pH 7.4, 50 mM

NaCl, 0.05 mM PMSF, 6 KIU7/ml aprotinin 0.5 mM DTT, 5% glycerol and 0.5% Triton X-100). Recombinant 6His-ErbB3 was purchased from Sigma. The in vitro binding assay was conducted by incubating 1 µg/ml recombinant ErbB3 with 1 µg/ml recombinant Rabaptin5 in a stringent buffer containing 50 mM Tris, pH 7.5, 150 mM NaCl, 1% NP40, 0.5% sodium deoxycholate, 0.1% SDS, 1 mM EDTA, HALT protease and phosphatase inhibitor overnight at 4°C. ErbB3 was immunoprecipitated and bound Rabaptin5 detected by immunoblotting.

Colocalization analysis

Analysis was conducted on confocal fluorescence images and analyzed using Image J. Rab4/11 and ErbB3 colocalization: Single Rab4 or Rab11 positive structures were identified and 40 × 40-pixel squares were drawn with the structures in the centre and saved as separate images. For each cell, a minimum of 15 structures were randomly selected and the intensity of the centre (7-pixel diameter circle, a) and the adjacent volume (background, b) for each structure was determined using ImageJ. These regions were subsequently transferred to the other channel (ErbB3) and similar measurements were performed. The relative enrichment of ErbB3 at the Rab-positive structures was determined by the formula (a-b)/b. An average for each cell was determined, and a minimum of 16 cells was analyzed for each condition. Images shown in the paper are average projections of all structures from all cells analyzed. ErbB3 and Integrin β1colocalization: Deconvoluted confocal image stacks were processed into maximum intensity projections using Fiji ImageJ. Signal intensities along manually drawn lines were obtained using the histogram tool. Colocalization was analyzed in image J as enrichment of Integrin β1 in ErbB3 positive structures (as described for ErbB3 and Rab colocalization above).

VSV-G trafficking assay

VSV-G ts045-GFP was expressed in MCF10A cells for 24 hours. Cells were incubated at 40°C for 6 hours, which causes misfolding and trapping of VSV-G in the ER. The cells were then shifted to permissive temperature (32°C) and either PFA-fixed at indicated times for immunofluorescence imaging or subjected to incubation on ice with Sulfo-NHS-SS-Biotin

(ThermoFisher Scientific) to biotinylate all surface proteins. Biotinylated cells were lysed in 1% Triton X-100 containing lysis buffer followed by pulldown with Streptavidin-agarose beads (Sigma) overnight and western blot analysis with indicated antibodies.

EdU incorporation assay

EdU incorporation into DNA of MCF10A monolayers subjected to a scratch assay in the presence of 1 µM lapatinib or vehicle alone was detected using the Click-iT EdU Alexa-488 Fluor Imaging kit (Invitrogen) following the manufacturer's instructions. Cells were later fixed, double stained with DAPI and mounted for microscopic imaging with a Zeiss Axio Imager M2. Quantification of EdU-positive cells at the indicated times in control or ErbB3-silenced cells was performed with ImageJ.

EV isolation and characterization

EV isolation and characterization was performed as previously described[49,50]. The cells were incubated for 48 hours in DMEM/F12 supplemented without horse serum as described above. The serum-free conditioned medium was centrifuged at 1,200 × g for 5 minutes to clear cell debris while measuring the corresponding number of cells. The medium supernatant was filtered through a 0.2 µm filter, was further concentrated 20× by tangential flow filtration on a 50 kDa Ultra-15 Centrifugal Filter (Amicon; Merck/Millipore) by centrifugation at 1,200 × g for 30 minutes, and defined as the VSF. EVs smaller than 200 nm were sub-fractionated based on the presence of the tetraspanin CD81 protein. VSF (150 µl) was incubated with 40 µL of anti-CD81-magnetic Dynabeads™ (#10616D, ThermoFisher Scientific) in 100 µl of 0.2 µm filtered PBS, respectively, for 60 minutes at 37°C. The magnetic beads containing CD81-EVs were immobilized, washed with PBS and the isolated EVs were stored at -20°C for up to 30 days. Additionally, conditioned media derived from MCF10A cells were first centrifuged at 1,200 × g to remove cell debris, and subsequently filtered through a 0.2 µm-filter (Sarstedt) and transferred to a polypropylene ultracentrifuge tube (Beckman Coulter). Ultracentrifugation

(UC) was carried out for 2 hours at 100.000 × g and 4ºC degrees in a swinging bucket rotor (SW28, Beckman Coulter).

Nanoparticle number and size distribution were measured through NTA (NanoSight system; Malvern Panalytical, equipped with a 532 nm laser and the NTA 3.4 analytic software). Three videos of 60 seconds each were recorded of each sample, using the following settings: camera level 8 and detection threshold 10. The system was calibrated with polystyrene beads of 100nm (Malvern). Modal diameter and per cell ratio of nanoparticles were analyzed statistically.

Transmission electron microscopy preparation was performed on freshly purified VSF or UC enriched EVs. The EVs were mixed with an equal volume of 4% w/v formaldehyde and further incubated with uranyl oxalate, pH 7.0, for 5 minutes, then stained in a drop containing 4% w/v uranyl acetate and 2% w/v methylcellulose on ice and protected from light for 10 minutes, as described[50]. Excess of UA/MC was removed by blotting on filter paper.

For immuno-gold staining, after the first 3 washes on PBS the protocol follows as indicated: sample was transferred to drops of 50mM Glycine in PBS for 3 × 1 minute. Then the sample was transferred to a drop of blocking solution, 1 % BSA in PBS, for 20 minutes. Primary and secondary incubations were carried out in 0.1% BSA in PBS for 40 minutes and washed away in 0.1 % BSA in PBS for 5 × 1 minute. Sample was then processed for TEM contrasting as described above. Dried grids were examined by TEM (FEI Tecnaii G2) operated at 80kV with an ORIUS SC200 CCD camera and Gatan Digital Micrograph software (both from Gatan Inc/Blue Scientific).

Cell viability assay

Cell viability was quantified using PrestoBlue Cell Viability Reagent (ThermoFisher Scientific) following the manufacturer's instructions. Briefly, 3×10^3 MCF10A cells were seeded into 96-well plates and incubated at 37˚C for 24 hours. Then, $1x10^9$ nanoparticles/mL of VSF enriched from cells transfected with siCtrl or siErbB3 was added to each well. Upon 48 hours

of treatment, 10 µl of PrestoBlue reagent was added to each well and fluorescence (540 nm excitation/ 590 nm emissions) was measured. The fluorescence units from VSF treated cells were normalized relative to those of vehicle-treated (EV-free media) and the graphs show average values of % viability with standard error of the mean (SEM) of at least three biological experiments.

Matrigel invasion assay

Transwell inserts (#351152) for 24-well plates (6.5 mm diameter, 8 µm pore) were coated with 300 µg/mL Matrigel matrix (#734-0269; both from Corning, New York City, NY, USA) diluted in coating buffer (10 mM Tris, pH 8.0, 0.7% w/v NaCl) and incubated at 37°C for 1 hour. MCF10A cells (5×10^4) treated with VSF (1×10^9 nanoparticles/mL) enriched from cells transfected with siCtrl or siErbB3, or with EV free media for 48 hours were seeded in DMEM/F12 in the upper chamber, while DMEM/F12 complete media was placed in the lower chamber and incubated at 37°C to induce the invasion through the Matrigel barrier for 16 hours. After incubation, the inserts were fixed in methanol and stained with 4′,6-diamidino-2-phenylindole (DAPI; Sigma-Aldrich AB, Stockholm, Sweden). Nuclei were counted in 10 pictures per insert, taken with the 20× objective, using ImageJ. Data were expressed as the percentage of invasion based on the ratio of the mean number of cells invading through Matrigel matrix per mean number of cells in the uncoated support.

Protein-protein interaction network analysis

A protein–protein interaction network for proteins interacting with GGA3 was constructed using the Search Tool for the Retrieval of Interacting Genes database (STRING-version 12.0; http://string-db.org/), with the required high confidence score (> 0.7).

Statistical analyses

All data, unless otherwise pointed out, are presented as the mean ± SEM, from the indicated independent biological experiments performed in triplicate or quintuplicate technical repeats.

Comparisons were performed using two-tailed paired Student's t-test or one-way ANOVA, followed by multiple paired comparisons conducted by means of the Tukey's or Bonferroni's post-test method when applicable. Additional statistical methods are explained in the respective figure legends. The data were analyzed with GraphPad Prism 10.1 (GraphPad Software, San Diego, CA). A p-value <0.05 was necessary to determine statistically significant differences.

References

1. Schlessinger, J. (2002). Ligand-induced, receptor-mediated dimerization and activation of EGF receptor. Cell *110*, 669–672.

2. Pradeep, S., Kim, S.W., Wu, S.Y., Nishimura, M., Chaluvally-Raghavan, P., Miyake, T., Pecot, C.V., Kim, S.-J., Choi, H.J., Bischoff, F.Z., et al. (2014). Hematogenous metastasis of ovarian cancer: rethinking mode of spread. Cancer Cell *26*, 77–91. https://doi.org/10.1016/j.ccr.2014.05.002.

3. Smirnova, T., Zhou, Z.N., Flinn, R.J., Wyckoff, J., Boimel, P.J., Pozzuto, M., Coniglio, S.J., Backer, J.M., Bresnick, A.R., Condeelis, J.S., et al. (2012). Phosphoinositide 3-kinase signaling is critical for ErbB3-driven breast cancer cell motility and metastasis. Oncogene *31*, 706–715. https://doi.org/10.1038/onc.2011.275.

4. Tiwary, S., Preziosi, M., Rothberg, P.G., Zeitouni, N., Corson, N., and Xu, L. (2014). ERBB3 is required for metastasis formation of melanoma cells. Oncogenesis *3*, e110. https://doi.org/10.1038/oncsis.2014.23.

5. Yoshioka, T., Nishikawa, Y., Ito, R., Kawamata, M., Doi, Y., Yamamoto, Y., Yoshida, M., Omori, Y., Kotanagi, H., Masuko, T., et al. (2010). Significance of integrin αvβ5 and erbB3 in enhanced cell migration and liver metastasis of colon carcinomas stimulated by hepatocyte-derived heregulin. Cancer Sci. *101*, 2011–2018. https://doi.org/10.1111/j.1349-7006.2010.01640.x.

6. Gaborit, N., Lindzen, M., and Yarden, Y. (2016). Emerging anti-cancer antibodies and combination therapies targeting HER3/ERBB3. Hum. Vaccines Immunother. *12*, 576–592. https://doi.org/10.1080/21645515.2015.1102809.

7. Al-Akhrass, H., Naves, T., Vincent, F., Magnaudeix, A., Durand, K., Bertin, F., Melloni, B., Jauberteau, M.-O., and Lalloué, F. (2017). Sortilin limits EGFR signaling by promoting its internalization in lung cancer. Nat. Commun. *8*, 1182. https://doi.org/10.1038/s41467-017-01172-5.

8. Avraham, R., and Yarden, Y. (2011). Feedback regulation of EGFR signalling: decision making by early and delayed loops. Nat. Rev. Mol. Cell Biol. *12*, 104–117. https://doi.org/10.1038/nrm3048.

9. Miaczynska, M., and Bar-Sagi, D. (2010). Signaling endosomes: seeing is believing. Curr. Opin. Cell Biol. *22*, 535–540. https://doi.org/10.1016/j.ceb.2010.05.007.

10. Sorkin, A., and Goh, L.K. (2009). Endocytosis and intracellular trafficking of ErbBs. Exp. Cell Res. *315*, 683–696.

11. Wiley, H.S. (2003). Trafficking of the ErbB receptors and its influence on signaling. Exp. Cell Res. *284*, 78–88.

12. Dietrich, M., Malik, M.S., Skeie, M., Bertelsen, V., and Stang, E. (2019). Protein kinase C regulates ErbB3 turnover. Exp. Cell Res. *382*, 111473. https://doi.org/10.1016/j.yexcr.2019.06.018.

13. Fosdahl, A.M., Dietrich, M., Schink, K.O., Malik, M.S., Skeie, M., Bertelsen, V., and Stang, E. (2017). ErbB3 interacts with Hrs and is sorted to lysosomes for degradation. Biochim. Biophys. Acta *1864*, 2241–2252. https://doi.org/10.1016/j.bbamcr.2017.08.011.

14. van Niel, G., Carter, D.R.F., Clayton, A., Lambert, D.W., Raposo, G., and Vader, P. (2022). Challenges and directions in studying cell-cell communication by extracellular vesicles. Nat. Rev. Mol. Cell Biol. *23*, 369–382. https://doi.org/10.1038/s41580-022-00460-3.

15. Raposo, G., and Stoorvogel, W. (2013). Extracellular vesicles: exosomes, microvesicles, and friends. J. Cell Biol. *200*, 373–383. https://doi.org/10.1083/jcb.201211138.

16. Bridgewater, R.E., Norman, J.C., and Caswell, P.T. (2012). Integrin trafficking at a glance. J. Cell Sci. *125*, 3695–3701. https://doi.org/10.1242/jcs.095810.

17. Tomas, A., Futter, C.E., and Eden, E.R. (2014). EGF receptor trafficking: consequences for signaling and cancer. Trends Cell Biol. *24*, 26–34. https://doi.org/10.1016/j.tcb.2013.11.002.

18. Lolo, F.-N., Pavón, D.M., Grande-García, A., Elosegui-Artola, A., Segatori, V.I., Sánchez, S., Trepat, X., Roca-Cusachs, P., and Del Pozo, M.A. (2022). Caveolae couple mechanical stress to integrin recycling and activation. eLife *11*, e82348. https://doi.org/10.7554/eLife.82348.

19. Arjonen, A., Alanko, J., Veltel, S., and Ivaska, J. (2012). Distinct recycling of active and inactive β1 integrins. Traffic Cph. Den. *13*, 610–625. https://doi.org/10.1111/j.1600-0854.2012.01327.x.

20. Crupi, M.J.F., Maritan, S.M., Reyes-Alvarez, E., Lian, E.Y., Hyndman, B.D., Rekab, A.N., Moodley, S., Antonescu, C.N., and Mulligan, L.M. (2020). GGA3-mediated recycling of the RET receptor tyrosine kinase contributes to cell migration and invasion. Oncogene *39*, 1361–1377. https://doi.org/10.1038/s41388-019-1068-z.

21. Parachoniak, C.A., Luo, Y., Abella, J.V., Keen, J.H., and Park, M. (2011). GGA3 functions as a switch to promote Met receptor recycling, essential for sustained ERK and cell migration. Dev. Cell *20*, 751–763. https://doi.org/10.1016/j.devcel.2011.05.007.

22. Puertollano, R., and Bonifacino, J.S. (2004). Interactions of GGA3 with the ubiquitin sorting machinery. Nat. Cell Biol. *6*, 244–251. https://doi.org/10.1038/ncb1106.

23. Ratcliffe, C.D.H., Sahgal, P., Parachoniak, C.A., Ivaska, J., and Park, M. (2016). Regulation of Cell Migration and β1 Integrin Trafficking by the Endosomal Adaptor GGA3. Traffic Cph. Den. *17*, 670–688. https://doi.org/10.1111/tra.12390.

24. Sahgal, P., Alanko, J., Icha, J., Paatero, I., Hamidi, H., Arjonen, A., Pietilä, M., Rokka, A., and Ivaska, J. (2019). GGA2 and RAB13 promote activity-dependent β1-integrin recycling. J. Cell Sci. *132*. https://doi.org/10.1242/jcs.233387.

25. Zhao, Y., and Keen, J.H. (2008). Gyrating clathrin: highly dynamic clathrin structures involved in rapid receptor recycling. Traffic Cph. Den. *9*, 2253–2264. https://doi.org/10.1111/j.1600-0854.2008.00819.x.

26. Mattera, R., Arighi, C.N., Lodge, R., Zerial, M., and Bonifacino, J.S. (2003). Divalent interaction of the GGAs with the Rabaptin-5-Rabex-5 complex. EMBO J. *22*, 78–88. https://doi.org/10.1093/emboj/cdg015.

27. Miller, G.J., Mattera, R., Bonifacino, J.S., and Hurley, J.H. (2003). Recognition of accessory protein motifs by the gamma-adaptin ear domain of GGA3. Nat. Struct. Biol. *10*, 599–606. https://doi.org/10.1038/nsb953.

28. Zhai, P., He, X., Liu, J., Wakeham, N., Zhu, G., Li, G., Tang, J., and Zhang, X.C. (2003). The interaction of the human GGA1 GAT domain with rabaptin-5 is mediated by residues on its three-helix bundle. Biochemistry *42*, 13901–13908. https://doi.org/10.1021/bi035392b.

29. Zhu, G., Zhai, P., Liu, J., Terzyan, S., Li, G., and Zhang, X.C. (2004). Structural basis of Rab5-Rabaptin5 interaction in endocytosis. Nat. Struct. Mol. Biol. *11*, 975–983. https://doi.org/10.1038/nsmb832.

30. de Renzis, S., Sönnichsen, B., and Zerial, M. (2002). Divalent Rab effectors regulate the sub-compartmental organization and sorting of early endosomes. Nat. Cell Biol. *4*, 124–133. https://doi.org/10.1038/ncb744.

31. Christoforides, C., Rainero, E., Brown, K.K., Norman, J.C., and Toker, A. (2012). PKD controls αvβ3 integrin recycling and tumor cell invasive migration through its substrate Rabaptin-5. Dev. Cell *23*, 560–572. https://doi.org/10.1016/j.devcel.2012.08.008.

32. Deneka, M., Neeft, M., Popa, I., van Oort, M., Sprong, H., Oorschot, V., Klumperman, J., Schu, P., and van der Sluijs, P. (2003). Rabaptin-5alpha/rabaptin-4 serves as a linker between rab4 and gamma(1)-adaptin in membrane recycling from endosomes. EMBO J. *22*, 2645–2657. https://doi.org/10.1093/emboj/cdg257.

33. Pagano, A., Crottet, P., Prescianotto-Baschong, C., and Spiess, M. (2004). In vitro formation of recycling vesicles from endosomes requires adaptor protein-1/clathrin and is regulated by rab4 and the connector rabaptin-5. Mol. Biol. Cell *15*, 4990–5000. https://doi.org/10.1091/mbc.E04-04-0355.

34. Sak, M.M., Breen, K., Rønning, S.B., Pedersen, N.M., Bertelsen, V., Stang, E., and Madshus, I.H. (2012). The oncoprotein ErbB3 is endocytosed in the absence of added ligand in a clathrin-dependent manner. Carcinogenesis *33*, 1031–1039. https://doi.org/10.1093/carcin/bgs128.

35. Sönnichsen, B., De Renzis, S., Nielsen, E., Rietdorf, J., and Zerial, M. (2000). Distinct membrane domains on endosomes in the recycling pathway visualized by multicolor imaging of Rab4, Rab5, and Rab11. J. Cell Biol. *149*, 901–914.

36. Weaver, V.M., Petersen, O.W., Wang, F., Larabell, C.A., Briand, P., Damsky, C., and Bissell, M.J. (1997). Reversion of the malignant phenotype of human breast cells in

three-dimensional culture and in vivo by integrin blocking antibodies. J. Cell Biol. *137*, 231–245. https://doi.org/10.1083/jcb.137.1.231.

37. Sun, L., Guo, S., Xie, Y., and Yao, Y. (2023). The characteristics and the multiple functions of integrin β1 in human cancers. J. Transl. Med. *21*, 787. https://doi.org/10.1186/s12967-023-04696-1.

38. Roberts, M., Barry, S., Woods, A., van der Sluijs, P., and Norman, J. (2001). PDGF-regulated rab4-dependent recycling of alphavbeta3 integrin from early endosomes is necessary for cell adhesion and spreading. Curr. Biol. CB *11*, 1392–1402.

39. Haskins, J.W., Nguyen, D.X., and Stern, D.F. (2014). Neuregulin 1–activated ERBB4 interacts with YAP to induce Hippo pathway target genes and promote cell migration. Sci. Signal. *7*, ra116–ra116. https://doi.org/10.1126/scisignal.2005770.

40. Wali, V.B., Haskins, J.W., Gilmore-Hebert, M., Platt, J.T., Liu, Z., and Stern, D.F. (2014). Convergent and Divergent Cellular Responses by ErbB4 Isoforms in Mammary Epithelial Cells. Mol. Cancer Res. *12*, 1140–1155. https://doi.org/10.1158/1541-7786.MCR-13-0637.

41. Nader, G.P.F., Ezratty, E.J., and Gundersen, G.G. (2016). FAK, talin and PIPKIγ regulate endocytosed integrin activation to polarize focal adhesion assembly. Nat. Cell Biol. *18*, 491–503. https://doi.org/10.1038/ncb3333.

42. Qu, F., Lorenzo, D.N., King, S.J., Brooks, R., Bear, J.E., and Bennett, V. (2016). Ankyrin-B is a PI3P effector that promotes polarized α5β1-integrin recycling via recruiting RabGAP1L to early endosomes. eLife *5*, e20417. https://doi.org/10.7554/eLife.20417.

43. Lauand, C., Rezende-Teixeira, P., Cortez, B.A., Niero, E.L. de O., and Machado-Santelli, G.M. (2013). Independent of ErbB1 gene copy number, EGF stimulates migration but is not associated with cell proliferation in non-small cell lung cancer. Cancer Cell Int. *13*, 38. https://doi.org/10.1186/1475-2867-13-38.

44. Maretzky, T., Evers, A., Zhou, W., Swendeman, S.L., Wong, P.-M., Rafii, S., Reiss, K., and Blobel, C.P. (2011). Migration of growth factor-stimulated epithelial and endothelial cells depends on EGFR transactivation by ADAM17. Nat. Commun. *2*, 229. https://doi.org/10.1038/ncomms1232.

45. Lindsay, A.J., Hendrick, A.G., Cantalupo, G., Senic-Matuglia, F., Goud, B., Bucci, C., and McCaffrey, M.W. (2002). Rab coupling protein (RCP), a novel Rab4 and Rab11 effector protein. J. Biol. Chem. *277*, 12190–12199. https://doi.org/10.1074/jbc.M108665200.

46. Woods, A.J., White, D.P., Caswell, P.T., and Norman, J.C. (2004). PKD1/PKCmu promotes alphavbeta3 integrin recycling and delivery to nascent focal adhesions. EMBO J. *23*, 2531–2543. https://doi.org/10.1038/sj.emboj.7600267.

47. Hirschberg, K., Miller, C.M., Ellenberg, J., Presley, J.F., Siggia, E.D., Phair, R.D., and Lippincott-Schwartz, J. (1998). Kinetic Analysis of Secretory Protein Traffic and Characterization of Golgi to Plasma Membrane Transport Intermediates in Living Cells. J. Cell Biol. *143*, 1485–1503.

48. Zhang, R., Bu, T., Cao, R., Li, Z., Wang, C., Huang, B., Wei, M., Yuan, L., and Yang, G. (2022). An optimized exosome production strategy for enhanced yield while without sacrificing cargo loading efficiency. J. Nanobiotechnology *20*, 463. https://doi.org/10.1186/s12951-022-01668-3.

49. Théry, C., Amigorena, S., Raposo, G., and Clayton, A. (2006). Isolation and characterization of exosomes from cell culture supernatants and biological fluids. Curr. Protoc. Cell Biol. *Chapter 3*, Unit 3.22. https://doi.org/10.1002/0471143030.cb0322s30.

50. Rodrigues-Junior, D.M., Tan, S.S., Lim, S.K., Leong, H.S., Melendez, M.E., Ramos, C.R.N., Viana, L. de S., Tan, D.S.W., Carvalho, A.L., Iyer, N.G., et al. (2019). Circulating extracellular vesicle-associated TGFβ3 modulates response to cytotoxic therapy in head and neck squamous cell carcinoma. Carcinogenesis *40*, 1452–1461. https://doi.org/10.1093/carcin/bgz148.

51. De Franceschi, N., Hamidi, H., Alanko, J., Sahgal, P., and Ivaska, J. (2015). Integrin traffic - the update. J. Cell Sci. *128*, 839–852. https://doi.org/10.1242/jcs.161653.

52. Hoshino, A., Costa-Silva, B., Shen, T.-L., Rodrigues, G., Hashimoto, A., Tesic Mark, M., Molina, H., Kohsaka, S., Di Giannatale, A., Ceder, S., et al. (2015). Tumour exosome integrins determine organotropic metastasis. Nature *527*, 329–335. https://doi.org/10.1038/nature15756.

53. Parachoniak, C.A., Luo, Y., Abella, J.V., Keen, J.H., and Park, M. (2011). GGA3 functions as a switch to promote Met receptor recycling, essential for sustained ERK and cell migration. Dev. Cell *20*, 751–763. https://doi.org/10.1016/j.devcel.2011.05.007.

54. Do, M.T., Chai, T.F., Casey, P.J., and Wang, M. (2017). Isoprenylcysteine carboxylmethyltransferase function is essential for RAB4A-mediated integrin β3 recycling, cell migration and cancer metastasis. Oncogene *36*, 5757–5767. https://doi.org/10.1038/onc.2017.183.

55. Ivaska, J., and Heino, J. (2011). Cooperation between integrins and growth factor receptors in signaling and endocytosis. Annu. Rev. Cell Dev. Biol. *27*, 291–320. https://doi.org/10.1146/annurev-cellbio-092910-154017.

56. Caswell, P.T., Vadrevu, S., and Norman, J.C. (2009). Integrins: masters and slaves of endocytic transport. Nat. Rev. Mol. Cell Biol. *10*, 843–853. https://doi.org/10.1038/nrm2799.

57. Li, J., Ballif, B.A., Powelka, A.M., Dai, J., Gygi, S.P., and Hsu, V.W. (2005). Phosphorylation of ACAP1 by Akt regulates the stimulation-dependent recycling of integrin beta1 to control cell migration. Dev. Cell *9*, 663–673. https://doi.org/10.1016/j.devcel.2005.09.012.

58. Caswell, P.T., Chan, M., Lindsay, A.J., McCaffrey, M.W., Boettiger, D., and Norman, J.C. (2008). Rab-coupling protein coordinates recycling of alpha5beta1 integrin and EGFR1 to promote cell migration in 3D microenvironments. J. Cell Biol. *183*, 143–155. https://doi.org/10.1083/jcb.200804140.

59. Reynolds, A.R., Hart, I.R., Watson, A.R., Welti, J.C., Silva, R.G., Robinson, S.D., Da Violante, G., Gourlaouen, M., Salih, M., Jones, M.C., et al. (2009). Stimulation of tumor growth and angiogenesis by low concentrations of RGD-mimetic integrin inhibitors. Nat. Med. *15*, 392–400. https://doi.org/10.1038/nm.1941.

60. Tan, X., Thapa, N., Sun, Y., and Anderson, R.A. (2015). A kinase-independent role for EGF receptor in autophagy initiation. Cell *160*, 145–160. https://doi.org/10.1016/j.cell.2014.12.006.

61. Ghossoub, R., Lembo, F., Rubio, A., Gaillard, C.B., Bouchet, J., Vitale, N., Slavík, J., Machala, M., and Zimmermann, P. (2014). Syntenin-ALIX exosome biogenesis and budding into multivesicular bodies are controlled by ARF6 and PLD2. Nat. Commun. *5*, 3477. https://doi.org/10.1038/ncomms4477.

62. Muralidharan-Chari, V., Clancy, J., Plou, C., Romao, M., Chavrier, P., Raposo, G., and D'Souza-Schorey, C. (2009). ARF6-regulated shedding of tumor cell-derived plasma membrane microvesicles. Curr. Biol. CB *19*, 1875–1885. https://doi.org/10.1016/j.cub.2009.09.059.

63. Jura, N., Endres, N.F., Engel, K., Deindl, S., Das, R., Lamers, M.H., Wemmer, D.E., Zhang, X., and Kuriyan, J. (2009). Mechanism for activation of the EGF receptor catalytic domain by the juxtamembrane segment. Cell *137*, 1293. https://doi.org/10.1016/j.cell.2009.04.025.

64. Littlefield, P., Liu, L., Mysore, V., Shan, Y., Shaw, D.E., and Jura, N. (2014). Structural analysis of the EGFR/HER3 heterodimer reveals the molecular basis for activating HER3 mutations. Sci. Signal. *7*, ra114–ra114. https://doi.org/10.1126/scisignal.2005786.

65. Yu, X., Miyamoto, S., and Mekada, E. (2000). Integrin alpha 2 beta 1-dependent EGF receptor activation at cell-cell contact sites. J. Cell Sci. *113 (Pt 12)*, 2139–2147.

66. Cao, Z., Wu, X., Yen, L., Sweeney, C., and Carraway, K.L. (2007). Neuregulin-induced ErbB3 downregulation is mediated by a protein stability cascade involving the E3 ubiquitin ligase Nrdp1. Mol. Cell. Biol. *27*, 2180–2188. https://doi.org/10.1128/MCB.01245-06.

67. Diamonti, A.J., Guy, P.M., Ivanof, C., Wong, K., Sweeney, C., and Carraway, K.L. (2002). An RBCC protein implicated in maintenance of steady-state neuregulin receptor levels. Proc. Natl. Acad. Sci. U. S. A. *99*, 2866–2871. https://doi.org/10.1073/pnas.052709799.

68. Qiu, X.-B., and Goldberg, A.L. (2002). Nrdp1/FLRF is a ubiquitin ligase promoting ubiquitination and degradation of the epidermal growth factor receptor family member, ErbB3. Proc. Natl. Acad. Sci. U. S. A. *99*, 14843–14848. https://doi.org/10.1073/pnas.232580999.

69. Pellinen, T., and Ivaska, J. (2006). Integrin traffic. J. Cell Sci. *119*, 3723–3731. https://doi.org/10.1242/jcs.03216.

70. Tang, Z., Kang, B., Li, C., Chen, T., and Zhang, Z. (2019). GEPIA2: an enhanced web server for large-scale expression profiling and interactive analysis. Nucleic Acids Res. *47*, W556–W560. https://doi.org/10.1093/nar/gkz430.

71. Lánczky, A., and Győrffy, B. (2021). Web-Based Survival Analysis Tool Tailored for Medical Research (KMplot): Development and Implementation. J. Med. Internet Res. *23*, e27633. https://doi.org/10.2196/27633.

72. Fekete, J.T., and Győrffy, B. (2019). ROCplot.org: Validating predictive biomarkers of chemotherapy/hormonal therapy/anti-HER2 therapy using transcriptomic data of 3,104 breast cancer patients. Int. J. Cancer *145*, 3140–3151. https://doi.org/10.1002/ijc.32369.

FIGURE LEGENDS

Figure 1. ErbB3 promotes Transferrin and Integrin β1 endocytic recycling. (**A**) Schematic outline of Transferrin recycling assays. (**B**) Confocal imaging of Alexa594-conjugated Transferrin chased with unlabelled holo-Transferrin for the indicated times in MCF7 cells. (**C**) Quantification of Alexa594 fluorescence intensity in cells treated as in **B** (n>17 cells for each data point from three experiments) normalized against the control siRNA treated, 0-hour timepoint of each independent experiment. (**D-G**) Confocal immunofluorescence imaging of traced surface labelled Integrin β1 and ErbB3: MCF7 cells were labelled on ice with an Alexa488-conjugated anti-Integrin β1 antibody prior to incubation for 30 minutes at 37ºC to allow Integrin β1 internalisation, and subsequent cell-fixation and immunolabelling of ErbB3 (red) and counterstaining with DAPI (blue). (**F**) Histogram of fluorescence intensities along dotted lines indicated in **E**. (**G**) Analysis of Integrin β1 and ErbB3 colocalization. Integrin β1 enrichment in ErbB3-positive intracellular structures (0.5-2 µm diameter) was determined by the formula (a-b)/b where a is the Integrin β1 intensity at ErbB3 positive structures, and b the adjacent intensity (background) for each structure. Average intensity projections of all analyzed structures are shown on the right-hand side. (**H**) Schematic outline of Integrin β1 recycling assays conducted in **I-N** after transfection with siRNA against the indicated targets. Integrin β1 surface-pool was labelled with an Alexa488-conjugated antibody and allowed to endocytose. Fluorophore label remaining on the cell surface was quenched with an anti-Alexa488 antibody, prior to visualisation of traced Integrin β1 re-emerging on the cell surface by live-cell TIRF microscopy. (**I**) Representative TIRF microscopy images of Integrin β1 from peripheral areas of MCF10A cells. (**J**) Quantifications of recycled Integrin β1 performed on indicated number of cells (outside of brackets on the right-hand side of graphs), from three independent experiments and shown as Alexa488 intensity normalized between 0-1, with the control as reference where $F_{norm}=((F_{max}-F_{min})/(F-F_{min}))$. (**K**) Representative TIRF microscopy images of Integrin β1 from prHMEC cells. (**L**) Quantifications of recycled Integrin β1 in prHMECs performed as described in **J**. (**M** and **N**) Quantified Integrin β1 recycling, after siRNA-mediated depletion of either EGFR (**M**) or ErbB2 (**N**). Data are presented as mean values ± SEM and p-

values determined by two-tailed paired Student's t-test. ns, non-significant. Scale bars, 10 µm (**A, D, E, I** and **K**) and 1 µm (**G**).

Figure 2. Ligand-independent role of ErbB3 in epithelial sheet motility. (**A-D**) Confocal immunofluorescence imaging of surface-labelled Integrin β1 (green) or actin (blue/black) on confluent sheets of MCF10A cells at 0 or 1 hour after labelling, as outlined in **A**. (**C**) Integrin β1 enrichment was determined as ((a-b)/b) where a = mean fluorescence intensity (Integrin β1) at a defined area of the leading edge (**C**) or cell-cell contact (**D**) and b=mean intensity of adjacent cytoplasm of the same area. Data are presented as mean values (>74 cells per data point) ± SEM, n=3 independent experiments. (**E**) Scratch closure assay of control or ErbB3-depleted MCF10A cells, cultured in serum-containing but growth factor-deprived media in the presence or absence of the EGFR/ErbB2 inhibitor lapatinib. Wound area highlighted in yellow. (**F** and **G**) Quantification of scratch aperture (**F**) or area under curve (AUC) (**G**) of samples treated as in (**E**) Data are presented as mean values ± SEM, n-values indicated in parenthesis. (**H**) Quantification of cell proliferation as incorporation of EdU for the indicated times in control or ErbB3 siRNA-transfected cells in the presence or absence of 1 µM lapatinib. Data presented as mean values ± SEM., n=3 independent experiments.

Figure 3. Loss of ErbB3 directs Integrin β1 for secretion as EV cargo. (**A**) Confocal imaging of ErbB3-mCherry and indicated Rab marker expressed in MCF7 cells, with or without prior treatment with the recycling inhibitor primaquine (PQ). (**B**) Analysis of ErbB3-mCherry colocalization with Rab4 or Rab11. The relative ErbB3 enrichment at the Rab-positive structures was determined by the formula (a-b)/b where a is the ErbB3-mCherry intensity of Rab4 structures centre, and b the adjacent volume (background) for each structure. Each data point represents the minimum average of 20 structures in one cell. P-values were determined using unpaired two-tailed Student's t-test. (**C**) Average projections of all analyzed (indicated number) of GFP-Rab4 or GFP-Rab11 positive structures from the indicated number of cells (3 independent experiments). (**D**) Experimental outline of the VSV-G trafficking experiments. (**E**)

Immunoblot analysis of the surface pool of VSV-G-ts45-GFP (pulldown of surface-biotinylated VSV-G-ts45-GFP), after its release from the endoplasmic reticulum (ER) at permissive temperature for the indicated times. (**F**) Quantification of VSV-G-GFP in biotin-pulldowns normalized levels as determined by immunoblot band intensities (n=3 independent experiments). (**G**) ErbB3 and β-Actin (as loading control) protein expression in MCF10A protein extracts of wild-type (WT) and transiently transfected cells with the indicated siRNAs. (**H**) Scheme of the EV enrichment protocol by (*i*) ultracentrifugation or (*ii*) tangential flow filtration, followed by CD81-immunoaffinity capture of EVs from conditioned media of breast epithelial cells. (**I**) EVs enriched in the VSF released by the indicated MCF10A cells were quantified by NTA in terms of nanoparticles modal size (nm) and number after normalization to the total cell number. (**J** and **K**) Protein expression levels of the indicated EV-specific proteins in EV extracts enriched as VSF (**J**) or CD81-EVs (**K**) derived from MCF10A cells transiently transfected with the indicated siRNAs; densitometric values were normalized to siRNA control. (**L**) Rab4A and GAPDH (as loading control) protein levels in MCF10A cells transiently transfected with the indicated siRNAs. (**M**) EVs enriched in the VSF released by MCF10A transiently transfected with the indicated siRNAs were quantified by NTA in terms of nanoparticles modal size (nm) and number upon normalization to the total cell number. Data presented as mean values ± SEM. P-values determined by two-tailed paired Student's t-test. *$p \leq 0.05$; **$p \leq 0.01$; ***$p \leq 0.001$; ns, non-significant.

Figure 4. ErbB3 loss directs Integrin β1 towards lysosomal degradation or EV secretion. (**A**) Schematic outline of traced internalised Integrin. (**B**) Confocal immunofluorescence imaging of traced internalised Integrin β1 in MCF10A cells. (**C**) Quantification of immunofluorescence intensity of internalised Integrin β1 traced for the indicated times (n>32 cells per data point from 5 independent experiments). (**D**) Determination of Integrin β1 turnover by pulse-chase metabolic labelling: Control or ErbB3 siRNA-transfected MCF10A cells were pulse-chase labelled with radioactive (^{35}S) methionine and cysteine. Radiolabelled Integrin β1 was visualized by radiography of immunoprecipitates (upper panel). Cell lysates and

immunoprecipitates were analyzed by immunoblotting. (**E**) Quantification of pulse chased ^{35}S-labelled Integrin β1 as in (**D**) (n=4 independent experiments). (**F** and **G**) Confocal immunofluorescence imaging of surface-labelled Integrin β1 (using an Alexa488-conjugated anti-Integrin β1 antibody), prior to (0 hour) or after tracing at 37°C for 1.5 hours. A scratch was inflicted prior to antibody incubation. Note that application of the lysosome inhibitor chloroquine caused Integrin β1 accumulation in intracellular vesicular compartments both in control or ErbB3-depleted cells. (**H**) Quantification of Integrin β1 fluorescence intensity in cells bordering the migratory front in samples treated as in **G**, showing that chloroquine restored Integrin β1 levels in ErbB3-depleted cells. Data were presented as mean values ± SEM., n=19-27 cells per data point from 3 independent experiments. P-values were determined by two-tailed paired Student's t-test. ns, non-significant. (**I**) Protein expression of ErbB3, Integrin β1 and the indicated EV-specific positive (Alix and TSG101) and negative (GM130) markers, besides β-Actin (as loading control) in the cell extract of MCF10A control or ErbB3-depleted samples. (**J**) Protein expression of Integrin β1 and the indicated EV-markers in the UC EV protein extract; densitometric values were normalized to siRNA control. (**K**) Representative TEM micrographs of EVs enriched by ultracentrifugation (UC EVs) from control or ErbB3-depleted MCF10A cells and stained with gold-conjugated anti-CD63 antibody (CD63-EVs are indicated by red arrows). (**K**) Cell viability assay measured with PrestoBlue Cell Viability Reagent in MCF10A cells incubated with EV free media as vehicle (Ctrl) or 1×10^9 nanoparticles of EVs secreted from MCF10A cells transiently transfected with control (VSF^{siCtrl}) or ErbB3-siRNA ($VSF^{siErbB3}$) for 48 hours. (**L**) Matrigel invasion assay in trans-wells with MCF10A cells stimulated with EV free media (Ctrl) or incubated with equal number of VSF^{siCtrl} or $VSF^{siErbB3}$ as described in K for 18 hours. The data in **L** and **M** are presented as mean values of three biological replicates ±SEM, in technical triplicates and p-values shown based on one-way ANOVA, followed by multiple paired comparisons conducted by means of Bonferroni's post-test method (**$p \leq 0.01$).

Figure 5. ErbB3 scaffolds assembly of the Arf6-GGA3-Rabaptin5 endosomal sorting complex. (**A**) Immunoblotting of ErbB3 immunoprecipitates or input cell lysates, after 30

minutes treatment with primaquine (PQ), showing endogenous binding of ErbB3 with GGA3 and Rabaptin5 that increases upon PQ treatment, and the presumed accumulation of recycling endosomes (representative of 3 independent experiments). (**B**) Immunoblotting of Arf6 immunoprecipitates or input cell lysates, transfected with the indicated siRNAs, following PQ or vehicle treatment for 10 minutes. (**C** and **D**) Quantification of GGA3 and Rabaptin5 protein levels (**C**: immunoblotting) and mRNA levels (**D**: RT-qPCR) in ErbB3 siRNA-transfected MCF10A cells relative to control cells (n=4 experiments for protein and n=3 for mRNA). Data are presented as mean values ± SEM. P-values determined by unpaired Student's t-test. (**E**) Structural model highlighting the putative GGA3-binding motif 864-DxxLL-867 in the ErbB3 kinase domain. (**F**) Immunoblotting of ErbB3 immunoprecipitates or input cell lysates, after ectopic expression of ErbB3 or the ErbB3 LL866/867AA mutant with GGA3 in HEK293T cells. (**G**) The LL866/867AA mutation compromises the ability of ErbB3 to promote assembly of the Arf6-GGA3-Rabaptin5 sorting complex: Immunoblotting of Arf6 immunoprecipitates or input cell lysates, following ectopic expression of Arf6, GGA3 and Rabaptin5 (Rbtn5), with or without ErbB3 or ErbB3-LL866/867AA.

Figure 6. Rabaptin5 and GGA3 are effectors of ErbB3 in endosomal trafficking. (**A**) Schematic outline of the Integrin β1 recycling assays in **B** and **C**. Re-emergence of traced internalised Integrin β1 on the cell surface was visualized by live-cell TIRF imaging, after prior transfection of control or Rabaptin5-targeting siRNA. (**B**) Quantification of recycled Integrin β1 was conducted on the indicated number of cells (right-hand side of graphs) from three independent experiments and shown as Alexa488 intensity normalized against levels at onset of tracing (0) and maximum intensity (1). (**C**) Columns show area under curves (AUC). (**D**) Determination of Integrin β1 turnover by pulse-chase metabolic labelling. Control or Rabaptin5 siRNA-transfected MCF10A cells were pulse-chase labelled with radioactive (^{35}S) methionine and cysteine. Radiolabelled Integrin β1 was visualized by radiography of Integrin β1 immunoprecipitates (upper panel). Cell lysates and immunoprecipitates were analyzed by immunoblotting as indicated. (**E**) Quantification of radiolabelled Integrin β1 at the indicated

times of three independent pulse and chase experiments. Data are presented as mean values ± SEM. P-values determined by two-tailed paired Student's t-test. ns, non-significant. (**F**) EVs enriched in the VSF released by the indicated MCF10A transiently transfected with control or Rabaptin5 siRNAs were quantified by NTA in terms of nanoparticles modal size (nm) and number after normalization to the total cell number. (**G**) Representative TEM micrographs of EVs enriched in the VSF of control or Rabaptin5-depleted MCF10A cells (EVs are indicated by red arrows). (**H**) Protein expression in the cell extract of MCF10A control samples, ErbB3- or GGA3-depleted (left panel) of ErbB3, Integrin β1, GGA3, besides the indicated EV-specific positive (ALIX, TSG101, CD81 and CD63) and GAPDH (as loading control). (**I**) EVs enriched by UC and released by the indicated MCF10A transiently transfected with control or GGA3 siRNAs were quantified by NTA in terms of nanoparticles modal size (nm) and number after normalization to the total cell number. Data in **F** and **I** are presented as mean values ± SEM. P-values were determined by unpaired Student's t-test. *$p \leq 0.05$. (**J**) Protein expression levels of Integrin β1 and the indicated positive and negative EV-markers in the UC EVs isolated from MCF10A cells described in **H**; densitometric values were normalized to siRNA control. (**K**) Representative TEM micrographs of EVs enriched by UC secreted from control, ErbB3- or GGA3-depleted MCF10A cells (EVs are indicated by red arrows).

SUPPLEMENTARY FIGURES AND LEGENDS

Supplementary Figure S1. ErbB3 gene expression in BRCA patients. (A) ErbB3 mRNA expression levels as log2-transformed transcripts per million (TPM) in tumor or corresponding normal tissue from TCGA datasets of BRCA. The data in the bottom indicates the number (N) of tissue samples analyzed in each group. Statistically significant differences are shown based on unpaired student's t-test. Red *p ≤ 0.01. **(B)** BRCA patient overall survival was calculated after sample stratification and compared with the Kaplan-Meier plotter database by auto select cut-off, based on the low and high expression level of ErbB3 mRNA. **(C)** BRCA patients were classified as chemotherapy non-responders or responders based on the relapse-free survival at five years post-treatment. The diagram presents median ErbB3 mRNA expression values, along with SEM and minimal and maximal values, as explained in the table below the graph, which also presents the number (N) of analyzed patients. Comparisons were performed using Mann–Whitney U-test (*p ≤ 0.05).

Supplementary Figure S2. ErbB3 promotes Integrin β1 endocytic recycling. (A, B) Columns show area under curve (AUC) of the Integrin β1 recycling data in MCF10A (**A**: related to Figure 1J) and prHMEC cells (**B**: related to Figure 1L). Data presented as mean values ± SEM. n-values indicated in main figures. **(C-F)** Immunofluorescence imaging of the surface pool of Integrin β1 labelled with Alexa488-conjugated antibody on ice for 1 hour, on MCF10A **(C, D)** or prHMEC cells **(E, F)** transfected with control (siCtrl) or ErbB3-targeting siRNAs. The columns in D and F show quantification of Integrin β1 fluorescence intensity, normalised against control siRNA treated samples. Data presented as mean ± SEM, from 6 independent experiments. ns, non-significant, as determined by unpaired Student's t-test.

Supplementary Figure S3. ErbB3 silencing does not affect Integrin β1 expression. (A) Immunoblotting analysis of the indicated proteins and a-Tubulin (as loading control) in the total MCF10A cell lysates under GF deprived culture conditions or upon supplementation of the

EGF and βNRG, after depletion of ErbB3, EGFR or ErbB2. **(B)** Immunoblotting analysis of ErbB3, Integrin β1 and GAPDH (as loading control) upon transfection of prHMEC cells with control or ErbB3 siRNA. **(C)** Relative levels of ErbB3 mRNA in control or ErbB3 siRNA transfected cells as determined by RT-qPCR (n=6 independent experiments). Data presented as mean ± SEM, from 6 independent experiments. ns, non-significant, as determined by unpaired Student's t-test.

Supplementary Figure S4. EGFR or ErbB2 does not promote Integrin β1 endocytic recycling. (**A**) Immunofluorescence imaging of the surface pool of Integrin β1 labelled with Alexa488-conjugated antibody on ice for 1 hour, on MCF10A cells transfected with control siRNA (siCtrl) or siRNAs targeting EGFR or ErbB2. **(B, C)** Quantification of Integrin β1 fluorescence intensity upon silencing of EGFR **(B)** or ErbB2 **(C)** and normalised against the respective control siRNA-treated samples. Data presented as mean values ± SEM. **(D)** Live-cell TIRF imaging of MCF10A cells to monitor recycling of labelled Integrin β1, after prior siRNA-mediated depletion of ErbB2, EGFR or ErbB3. **(E)** Related to the Figures 1M and 1N: shows AUC of the Integrin β1 recycling data (Figures 1M and 1N). Data presented as mean values ± SEM. n-values indicated in main figures. n-values indicated in main figures (Figures 1M and 1N).

Supplementary Figure S5. ErbB3 promotes endocytic recycling of Integrin β1 in absence of detectable tyrosine kinase signalling. (A, B) Expression of siRNA-resistant ErbB3 restores the surface pool of traced Integrin β1 in ErbB3-depleted MCF10 cells. **(A)** Confocal imaging of Integrin β1 labelled on the cell surface with an Alexa488-conjugated antibody, prior to (0 hour) or after tracing (1 hour), on cells expressing siRNA-resistant mCh-ErbB3 or fluorophore alone with or without transfection of control (siCtrl) or ErbB3 siRNA as indicated. **(B)** Fluorescence-intensity (Integrin β1) along cell-cell borders was quantified from 3 independent experiments. Values were normalised against intensities prior to tracing (0 hour). The results suggest that off-target effects of the ErbB3 siRNAs do not underlie the

observed recycling defect. Data presented as mean values ± SD, n>230 cell-cell borders from 3 independent experiments and p values determined by two-tailed paired Student's t-test. **(C)** Immunoblotting analysis of ErbB3 immunoprecipitates or total cell lysates of MCF10A cells cultured in the presence of 5% horse serum or under growth factor (GF) deprived. Antibodies detecting total phospho-tyrosine (4G10; pTyr) or the specific phospho-tyrosine 1289 on ErbB3 were used and α-Tubulin was used as loading control for the total cell lysates.

Supplementary Figure S6 ErbB3 does not regulate exocytic trafficking of VSV-G from the ER. (A) Immunoblotting analysis of isolated surface-biotinylated VSV-G-ts45-GFP, following its temperature-dependent release from the endoplasmic reticulum (ER) for 2 hours in MCF7 cells. Note that ErbB3-depletion does not influence the emergence of VSV-G at the plasma membrane. **(B)** Confocal imaging of VSV-G-ts45-GFP (green) and markers of the TGN (GM130; blue) and the cell surface (E-cadherin; red) in control or ErbB3 siRNA transfected MCF7 cells at non-permissive temperature (40°C) and following its subsequent shift to permissive (32°C) temperature. Note that VSV-G-ts45-GFP localises to the ER at 40°C, while after 30 minutes at permissive temperature most of the VSV-G-ts45-GFP has moved to the TGN and after 1 hour to the cell surface, both in the presence or absence of ErbB3.

Supplementary Figure S7. Loss of ErbB3 induces EV release. (A) Representative TEM micrographs of EVs enriched in the VSF of control or ErbB3-depleted MCF10A cells (EVs are indicated by red arrows). **(B)** Representative nanoparticle traces measured through NTA. The VSF from MCF10A transiently transfected or not (WT) with control siRNA (siCtrl) or independent ErbB3 siRNAs were analyzed by Nanoparticles Tracking Analysis (NTA) 3.4 software, according to the manufacturer's protocol. 100nm beads were used as a positive control. **(C)** CD63 protein expression level in EV extracts enriched by UC derived from MCF10A cells transiently transfected with the indicated siRNAs; densitometric values were normalized to siRNA control. **(D)** ErbB3 and β-Actin (as loading control) protein levels in prHMEC cells transiently transfected with the indicated siRNAs. **(E)** EVs enriched in the VSF

released by prHMEC transiently transfected with the indicated siRNAs were quantified by NTA in terms of nanoparticles modal size (nm) and number upon normalization to the total cell number. Data presented as mean values ± SEM. P-values determined by unpaired Student's t-test. *p ≤ 0.05.

Supplementary Figure S8. Integrin β1 stability is reduced upon depletion of ErbB3. (A) Immunoblotting analysis of the indicated proteins and GAPDG (as loading control) in MCF10A cells, transfected with control (siCtrl) or ErbB3 siRNA prior to treatment with protein synthesis inhibitor cycloheximide (CHX) or vehicle alone for the indicated times in hours. **(B)** Quantification of Integrin β1 band intensities presented as mean values ± SEM, n=3 independent experiments and p-values determined by two-tailed paired Student's t-test.

Supplementary Figure S9. ErbB3 binds to Rabaptin5 in vitro and promotes its stability. (A) GGA3 protein-protein interaction network analysis using STRING and a confidence score > 0.7. The protein RABEP1 is Rabaptin5 and its annotation is clarified in the diagram. **(B)** Immunoblotting analysis of MCF10A cells, transfected with control (siCtrl) or ErbB3 siRNA prior to treatment with the proteasome inhibitor MG132 for the indicated times in hours. MG321 partially restores GGA3 and Rabaptin5 levels in ErbB3-depleted cells. **(C)** In vitro binding of ErbB3 to Rabaptin5. Immunoblotting of ErbB3-immunoprecipitates following incubation of recombinant ErbB3 and Rabaptin5.

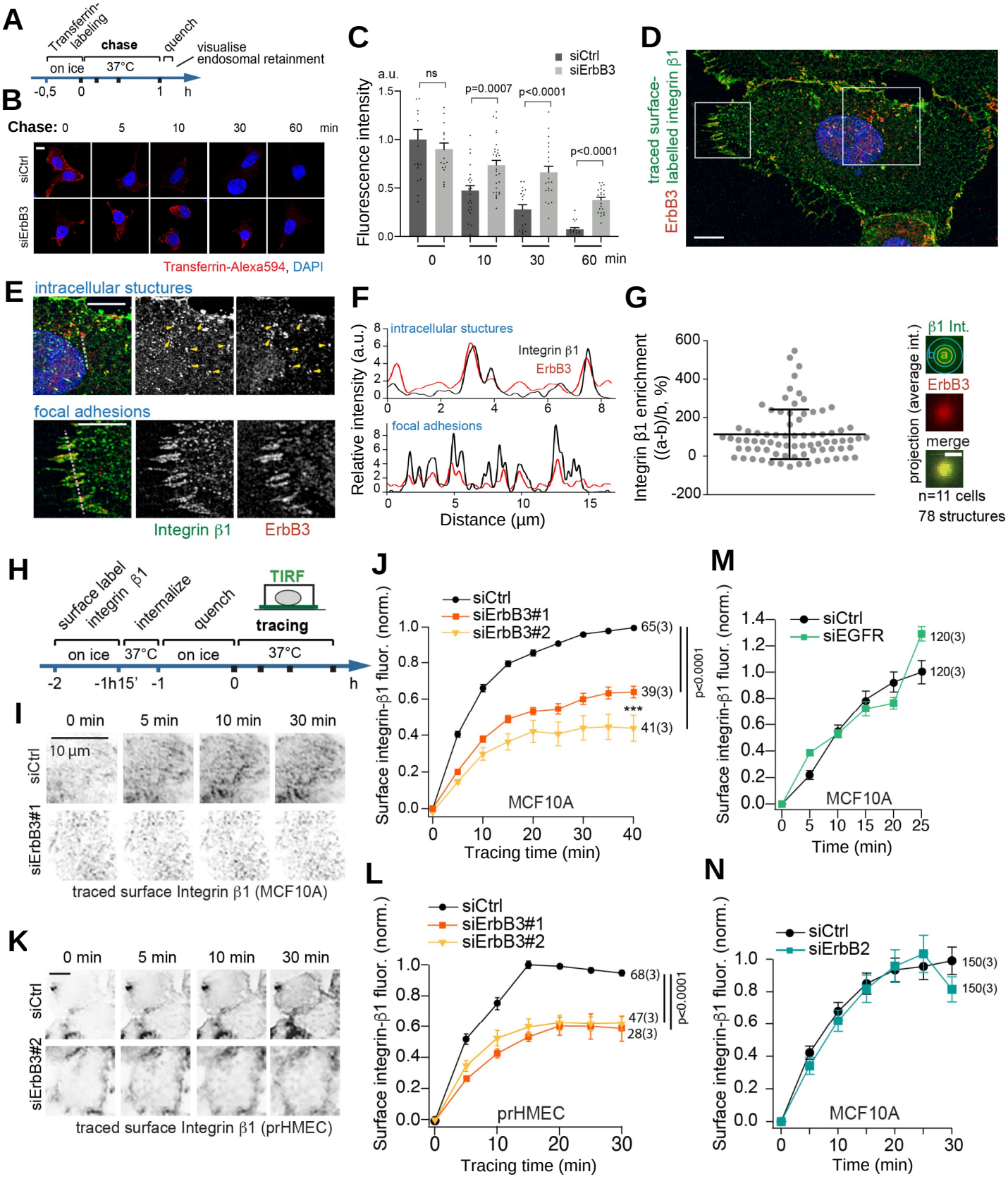
A
Transferrin-labeling
chase
quench
visualise endosomal retainment
on ice
37°C
-0,5
0
1
h
B
Chase: 0
5
10
30
60
min
siCtrl
siErbB3
Transferrin-Alexa594, DAPI
C
siCtrl
siErbB3
a.u.
ns
p=0.0007
p<0.0001
p<0.0001
Fluorescence intensity
0
10
30
60
min
D
traced surface-labelled integrin β1
ErbB3
E
intracellular stuctures
focal adhesions
Integrin β1
ErbB3
F
intracellular stuctures
Integrin β1
ErbB3
focal adhesions
Relative intensity (a.u.)
Distance (µm)
G
Integrin β1 enrichment ((a-b)/b, %)
β1 Int.
ErbB3
merge
projection (average int.)
n=11 cells
78 structures
H
surface label integrin β1
internalize
quench
TIRF
tracing
on ice
37°C
on ice
37°C
-2
-1h15'
-1
0
h
I
0 min
5 min
10 min
30 min
10 µm
siCtrl
siErbB3#1
traced surface Integrin β1 (MCF10A)
J
siCtrl
siErbB3#1
siErbB3#2
65(3)
39(3)
41(3)
***
p<0.0001
MCF10A
Surface integrin-β1 fluor. (norm.)
Tracing time (min)
K
0 min
5 min
10 min
30 min
siCtrl
siErbB3#2
traced surface Integrin β1 (prHMEC)
L
siCtrl
siErbB3#1
siErbB3#2
68(3)
47(3)
28(3)
p<0.0001
prHMEC
Surface integrin-β1 fluor. (norm.)
Tracing time (min)
M
siCtrl
siEGFR
120(3)
120(3)
MCF10A
Surface integrin-β1 fluor. (norm.)
Time (min)
N
siCtrl
siErbB2
150(3)
150(3)
MCF10A
Surface integrin-β1 fluor. (norm.)
Time (min)

Figure 1

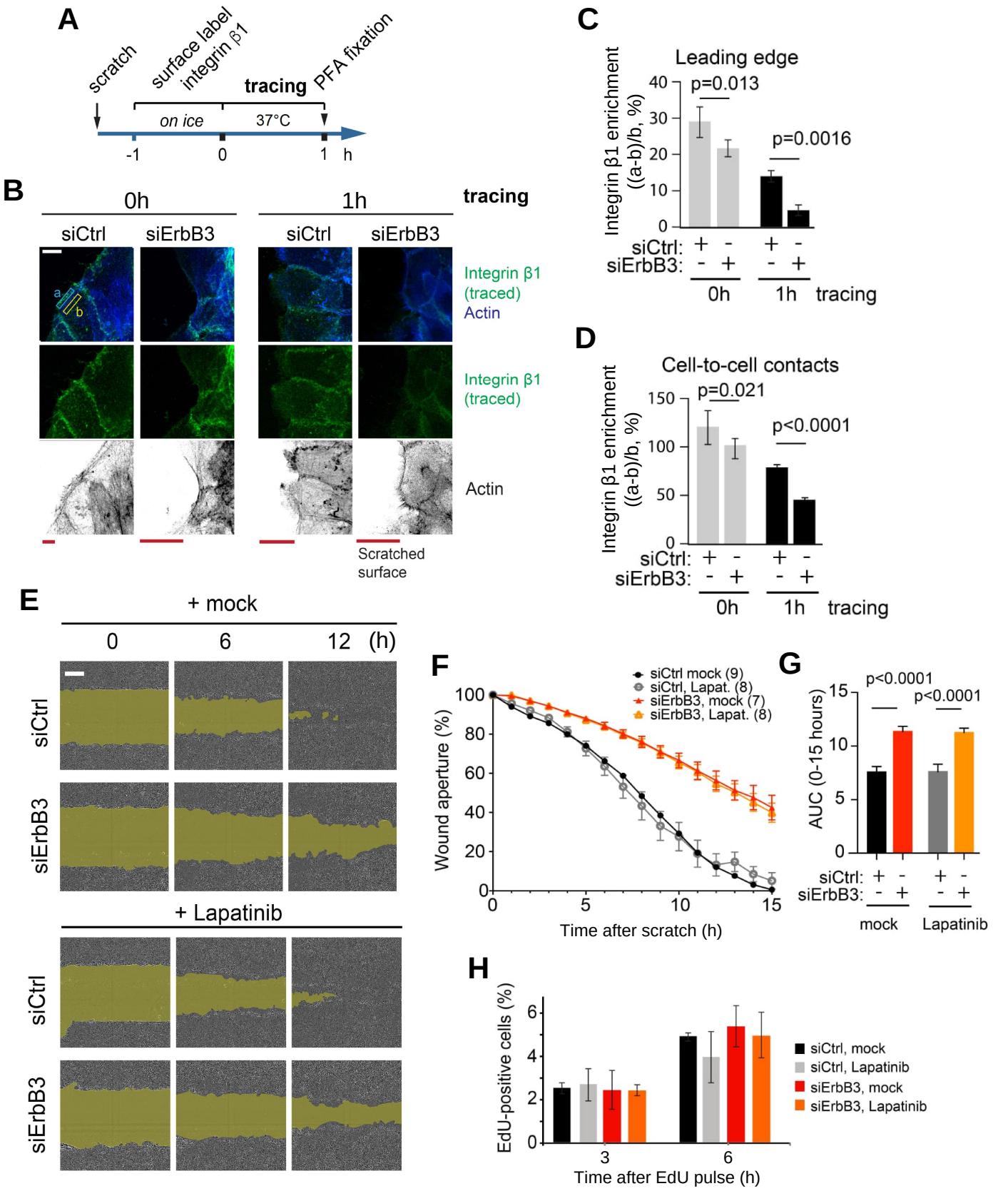
A
scratch
surface label integrin β1
tracing
PFA fixation
on ice
37°C
-1
0
1
h
B
0h
1h
tracing
siCtrl
siErbB3
siCtrl
siErbB3
a
b
Integrin β1 (traced)
Actin
Integrin β1 (traced)
Actin
Scratched surface
C
Leading edge
Integrin β1 enrichment ((a-b)/b, %)
p=0.013
p=0.0016
siCtrl: + - + -
siErbB3: - + - +
0h
1h
tracing
D
Cell-to-cell contacts
Integrin β1 enrichment ((a-b)/b, %)
p=0.021
p<0.0001
siCtrl: + - + -
siErbB3: - + - +
0h
1h
tracing
E
+ mock
0
6
12
(h)
siCtrl
siErbB3
+ Lapatinib
siCtrl
siErbB3
F
siCtrl mock (9)
siCtrl, Lapat. (8)
siErbB3, mock (7)
siErbB3, Lapat. (8)
Wound aperture (%)
Time after scratch (h)
G
p<0.0001
p<0.0001
AUC (0-15 hours)
siCtrl: + - + -
siErbB3: - + - +
mock
Lapatinib
H
EdU-positive cells (%)
siCtrl, mock
siCtrl, Lapatinib
siErbB3, mock
siErbB3, Lapatinib
Time after EdU pulse (h)

Figure 2

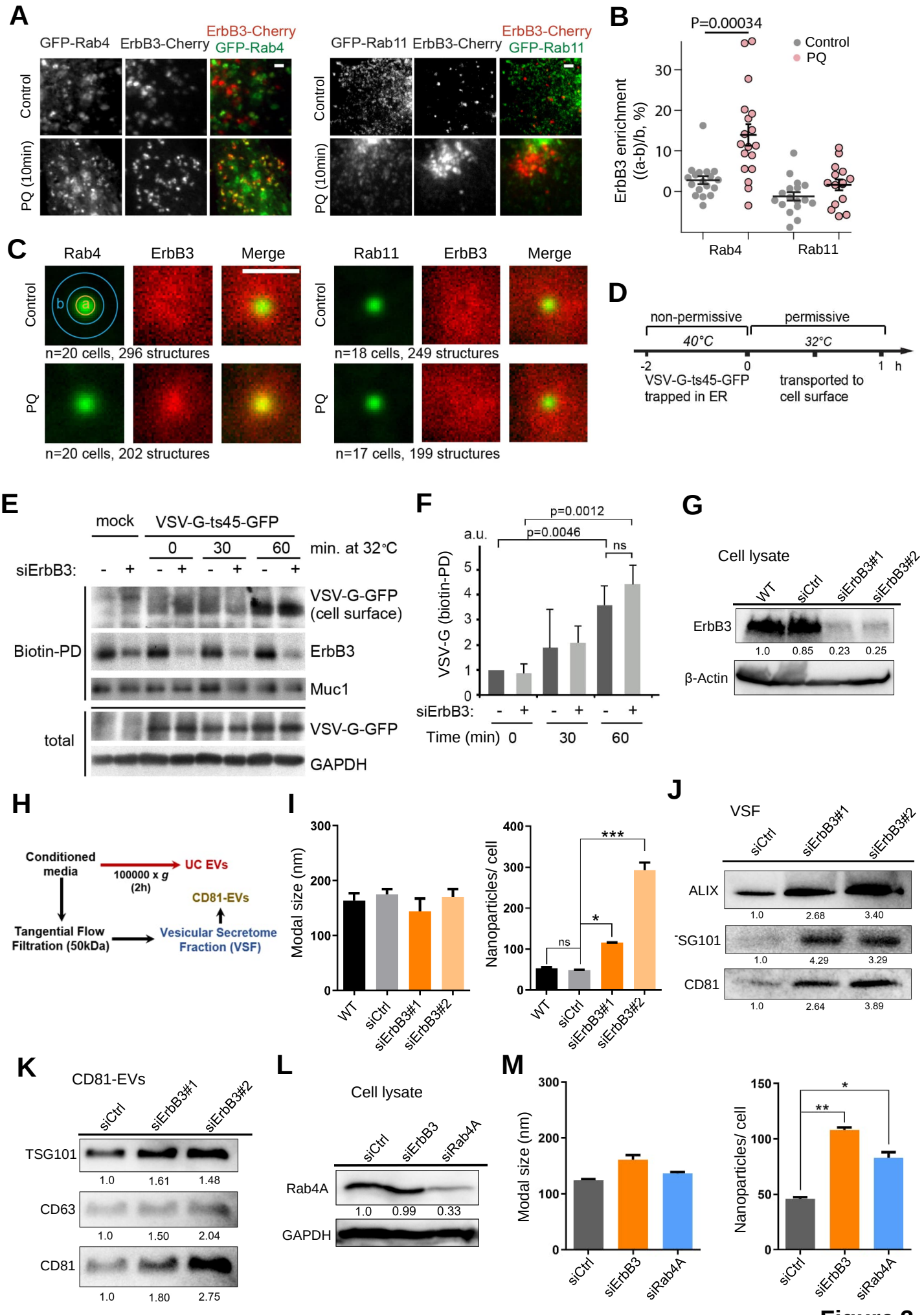
A
GFP-Rab4
ErbB3-Cherry
ErbB3-Cherry GFP-Rab4
GFP-Rab11
ErbB3-Cherry GFP-Rab11
Control
PQ (10min)
B
P=0.00034
Control
PQ
ErbB3 enrichment ((a-b)/b, %)
Rab4
Rab11
C
Rab4
ErbB3
Merge
Rab11
n=20 cells, 296 structures
n=18 cells, 249 structures
n=20 cells, 202 structures
n=17 cells, 199 structures
PQ
D
non-permissive
permissive
40°C
32°C
VSV-G-ts45-GFP trapped in ER
transported to cell surface
E
mock
VSV-G-ts45-GFP
min. at 32°C
siErbB3:
Biotin-PD
total
VSV-G-GFP (cell surface)
ErbB3
Muc1
VSV-G-GFP
GAPDH
F
p=0.0012
p=0.0046
ns
a.u.
VSV-G (biotin-PD)
siErbB3:
Time (min)
G
Cell lysate
WT
siCtrl
siErbB3#1
siErbB3#2
ErbB3
β-Actin
1.0
0.85
0.23
0.25
H
Conditioned media
UC EVs
100000 x g (2h)
CD81-EVs
Tangential Flow Filtration (50kDa)
Vesicular Secretome Fraction (VSF)
I
Modal size (nm)
Nanoparticles/ cell
ns
*
***
J
VSF
ALIX
TSG101
CD81
1.0
2.68
3.40
1.0
4.29
3.29
1.0
2.64
3.89
K
CD81-EVs
TSG101
CD63
CD81
1.0
1.61
1.48
1.0
1.50
2.04
1.0
1.80
2.75
L
Cell lysate
siCtrl
siErbB3
siRab4A
Rab4A
GAPDH
1.0
0.99
0.33
M
Modal size (nm)
Nanoparticles/ cell
**
*

Figure 3

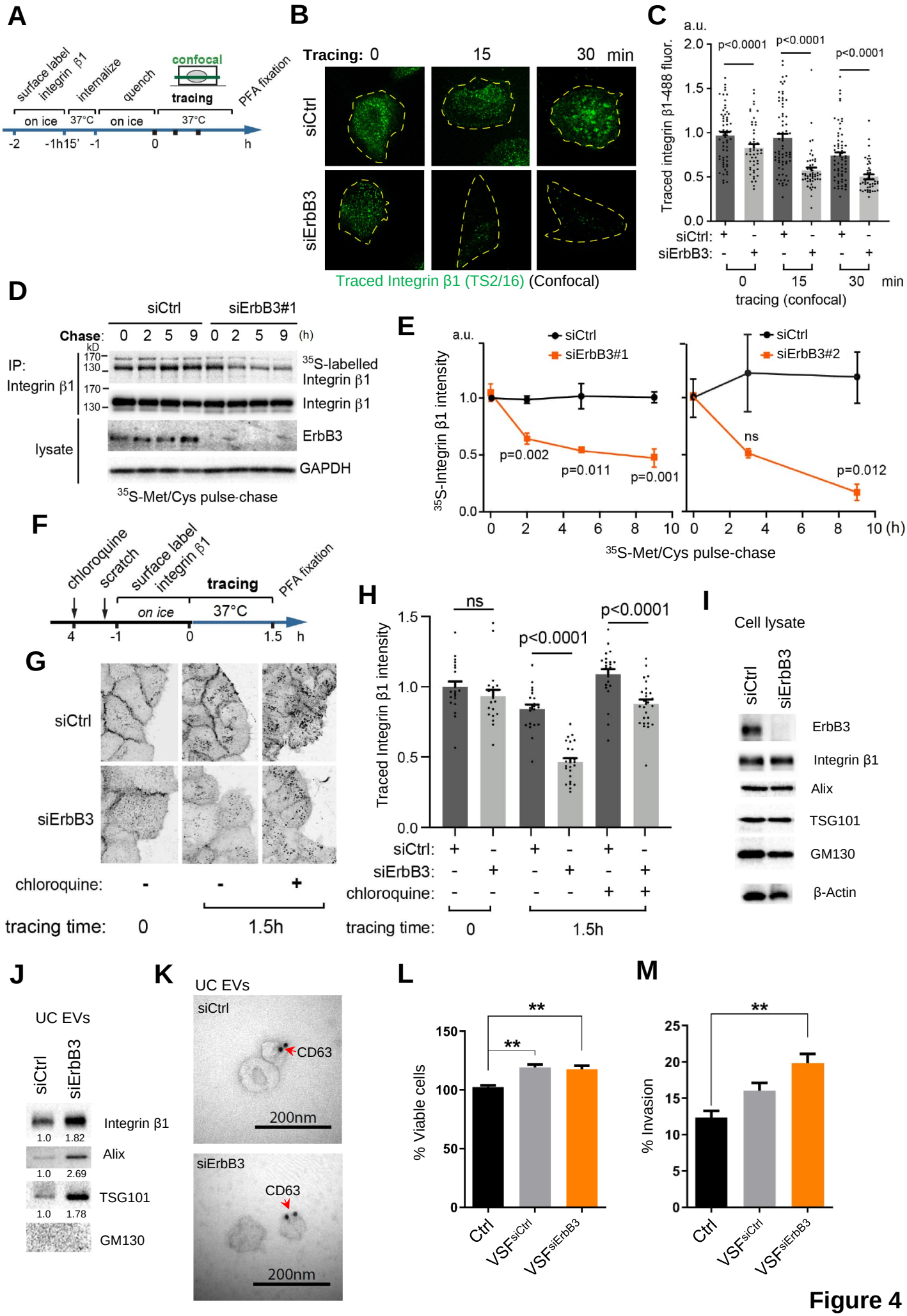
A
surface label integrin β1
internalize
quench
confocal
tracing
PFA fixation
on ice
37°C
on ice
37°C
-2
-1h15'
-1
0
h
B
Tracing: 0
15
30 min
siCtrl
siErbB3
Traced Integrin β1 (TS2/16) (Confocal)
C
a.u.
Traced integrin β1-488 fluor.
p<0.0001
p<0.0001
p<0.0001
siCtrl:
siErbB3:
0
15
30 min
tracing (confocal)
D
siCtrl
siErbB3#1
Chase: 0 2 5 9 0 2 5 9 (h)
kD
IP: Integrin β1
35S-labelled Integrin β1
Integrin β1
lysate
ErbB3
GAPDH
35S-Met/Cys pulse-chase
E
a.u.
siCtrl
siErbB3#1
siCtrl
siErbB3#2
35S-Integrin β1 intensity
p=0.002
p=0.011
p=0.001
ns
p=0.012
35S-Met/Cys pulse-chase
(h)
F
chloroquine
scratch
surface label integrin β1
tracing
PFA fixation
on ice
37°C
4
-1
0
1.5
h
G
siCtrl
siErbB3
chloroquine:
tracing time: 0
1.5h
H
Traced Integrin β1 intensity
ns
p<0.0001
p<0.0001
siCtrl:
siErbB3:
chloroquine:
tracing time: 0
1.5h
I
Cell lysate
siCtrl
siErbB3
ErbB3
Integrin β1
Alix
TSG101
GM130
β-Actin
J
UC EVs
siCtrl
siErbB3
Integrin β1
1.0 1.82
Alix
1.0 2.69
TSG101
1.0 1.78
GM130
K
UC EVs
siCtrl
CD63
200nm
siErbB3
CD63
200nm
L
% Viable cells
**
**
Ctrl
VSFsiCtrl
VSFsiErbB3
M
% Invasion
**
Ctrl
VSFsiCtrl
VSFsiErbB3

Figure 4

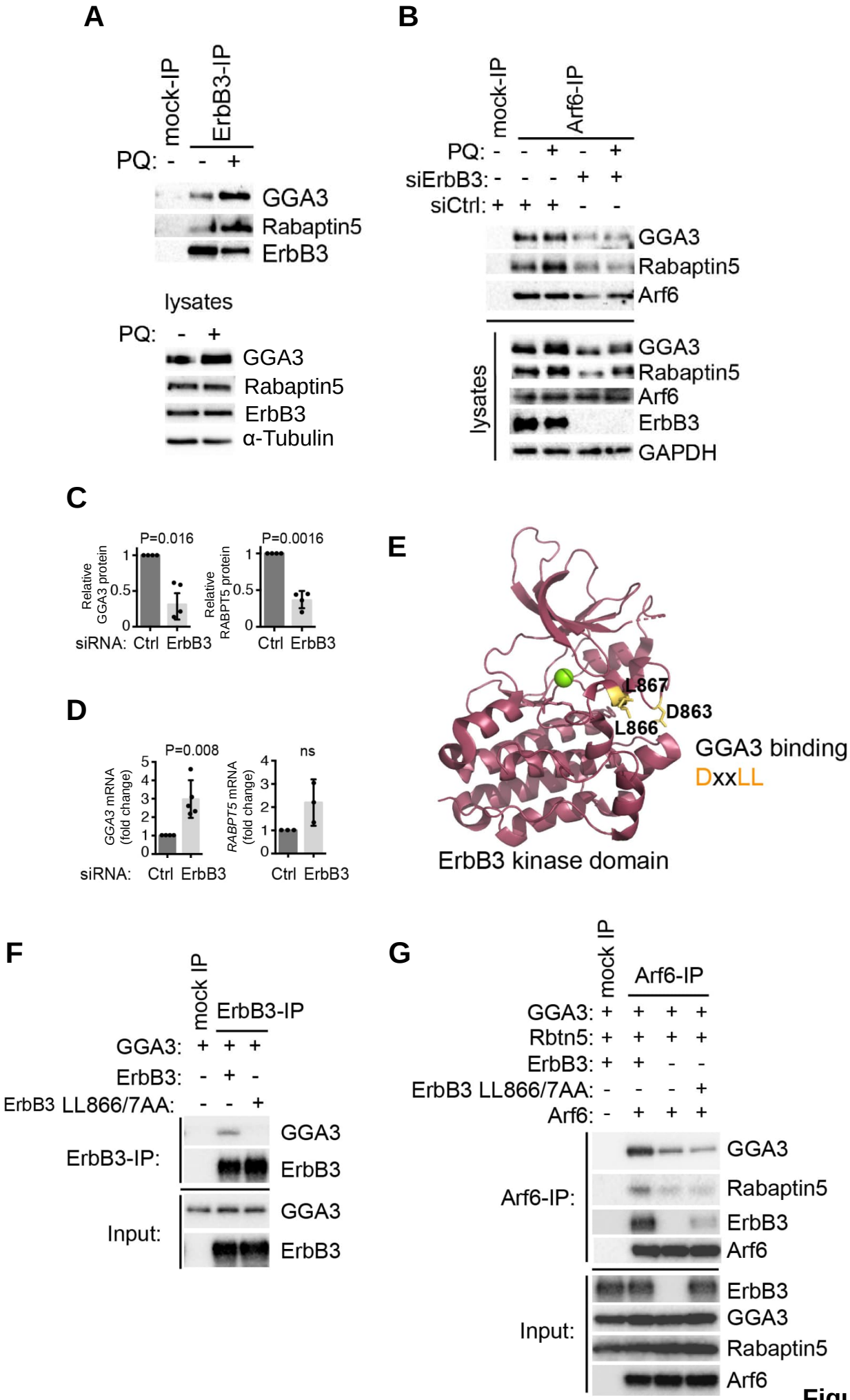
A
mock-IP
ErbB3-IP
PQ: - - +
GGA3
Rabaptin5
ErbB3
lysates
PQ: - +
GGA3
Rabaptin5
ErbB3
α-Tubulin
B
mock-IP
Arf6-IP
PQ: - - + - +
siErbB3: - - - + +
siCtrl: + + + - -
GGA3
Rabaptin5
Arf6
lysates
GGA3
Rabaptin5
Arf6
ErbB3
GAPDH
C
P=0.016
Relative GGA3 protein
P=0.0016
Relative RABPT5 protein
siRNA: Ctrl ErbB3 Ctrl ErbB3
D
P=0.008
GGA3 mRNA (fold change)
ns
RABPT5 mRNA (fold change)
siRNA: Ctrl ErbB3 Ctrl ErbB3
E
L867
D863
L866
GGA3 binding
DxxLL
ErbB3 kinase domain
F
mock IP
ErbB3-IP
GGA3: + + +
ErbB3: - + -
ErbB3 LL866/7AA: - - +
ErbB3-IP:
GGA3
ErbB3
Input:
GGA3
ErbB3
G
mock IP
Arf6-IP
GGA3: + + + +
Rbtn5: + + + +
ErbB3: + + - -
ErbB3 LL866/7AA: - - - +
Arf6: - + + +
Arf6-IP:
GGA3
Rabaptin5
ErbB3
Arf6
Input:
ErbB3
GGA3
Rabaptin5
Arf6

Figure 5

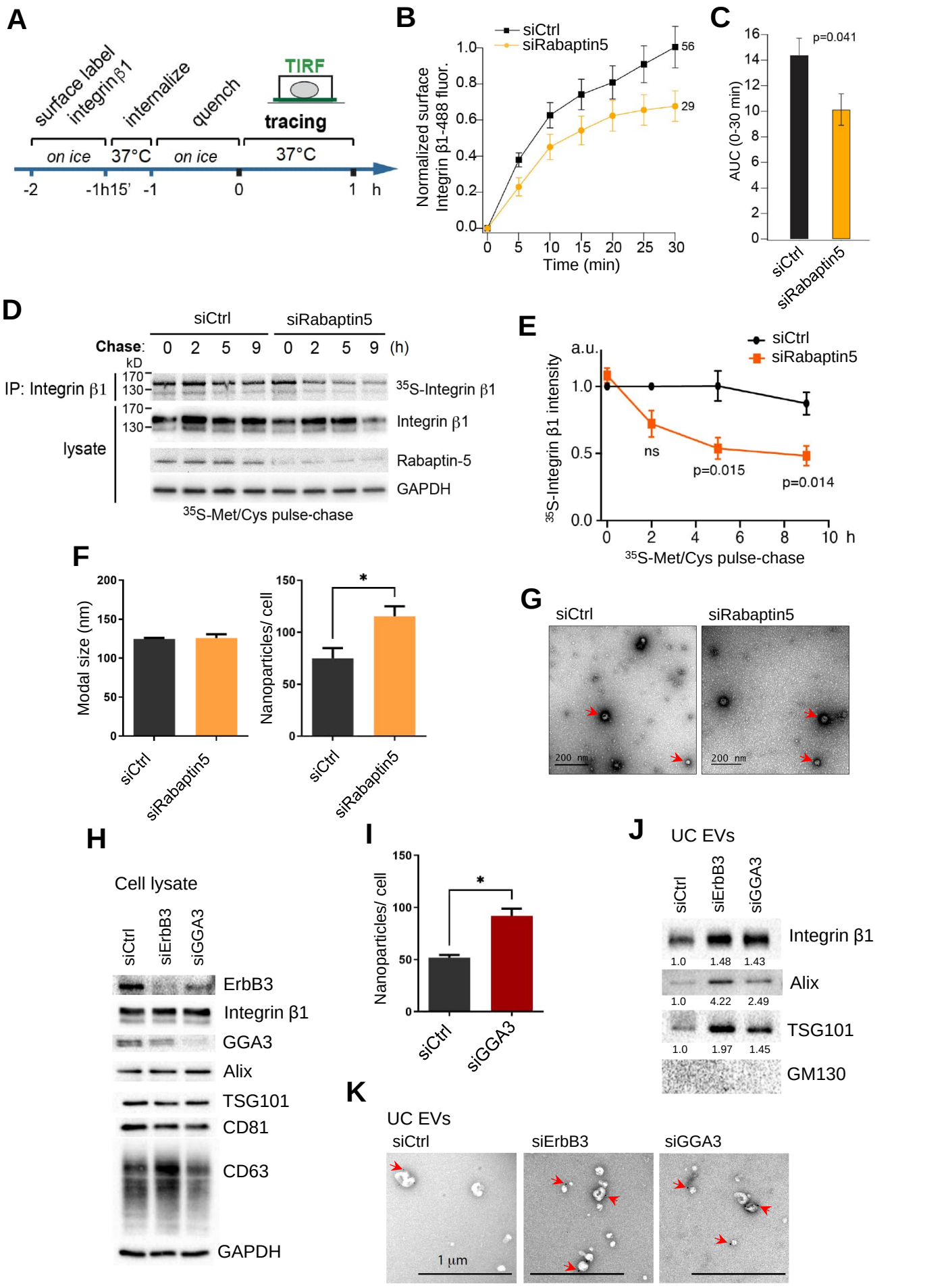
A
surface label integrin β1
internalize
quench
TIRF
tracing
on ice
37°C
on ice
37°C
-2
-1h15'
-1
0
1
h
B
siCtrl
siRabaptin5
Normalized surface Integrin β1-488 fluor.
Time (min)
56
29
C
p=0.041
AUC (0-30 min)
siCtrl
siRabaptin5
D
siCtrl
siRabaptin5
Chase: 0 2 5 9 0 2 5 9 (h)
kD
IP: Integrin β1
35S-Integrin β1
lysate
Integrin β1
Rabaptin-5
GAPDH
35S-Met/Cys pulse-chase
E
siCtrl
siRabaptin5
a.u.
35S-Integrin β1 intensity
ns
p=0.015
p=0.014
35S-Met/Cys pulse-chase
F
Modal size (nm)
Nanoparticles/ cell
siCtrl
siRabaptin5
G
siCtrl
siRabaptin5
200 nm
H
Cell lysate
siCtrl
siErbB3
siGGA3
ErbB3
Integrin β1
GGA3
Alix
TSG101
CD81
CD63
GAPDH
I
Nanoparticles/ cell
siCtrl
siGGA3
J
UC EVs
siCtrl
siErbB3
siGGA3
Integrin β1
1.0 1.48 1.43
Alix
1.0 4.22 2.49
TSG101
1.0 1.97 1.45
GM130
K
UC EVs
siCtrl
siErbB3
siGGA3
1 µm

Figure 6

A

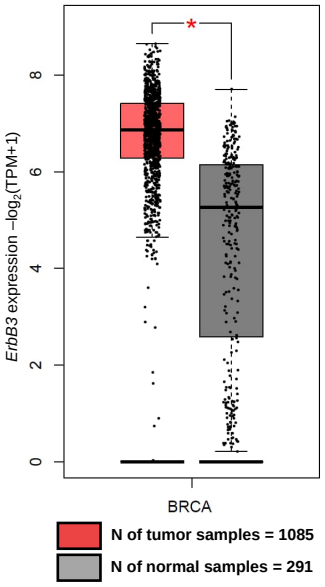

B

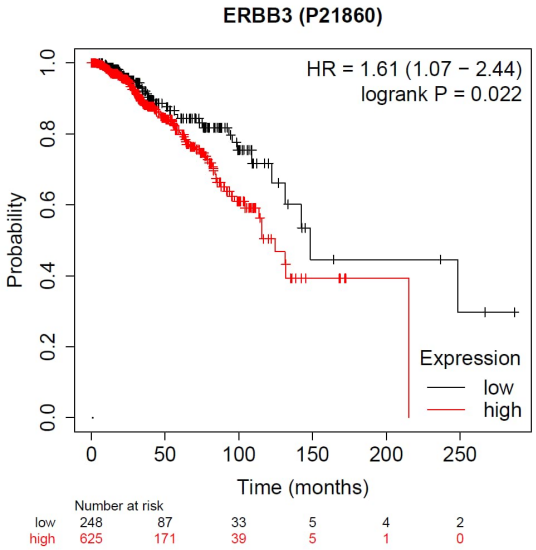

C

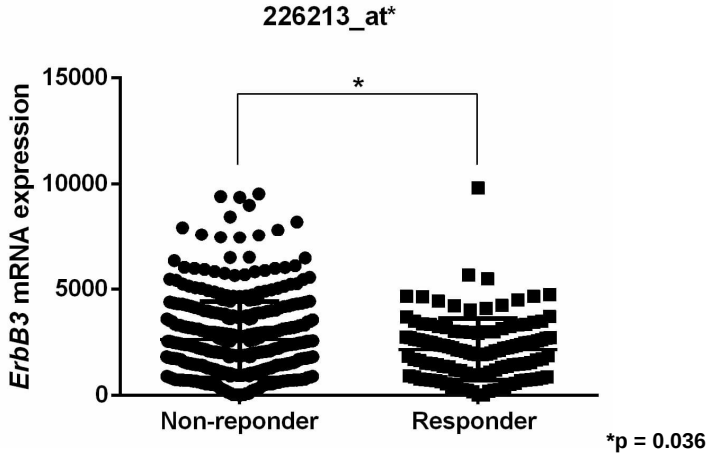

Chemotherapy response	N of patients	Mean	SD	Median	Minimum	Maximum
Non-Responder	119	2174	1460	2097	26	9819
Responder	388	2631	1803	2279	27	9539

Suppl. Figure S1

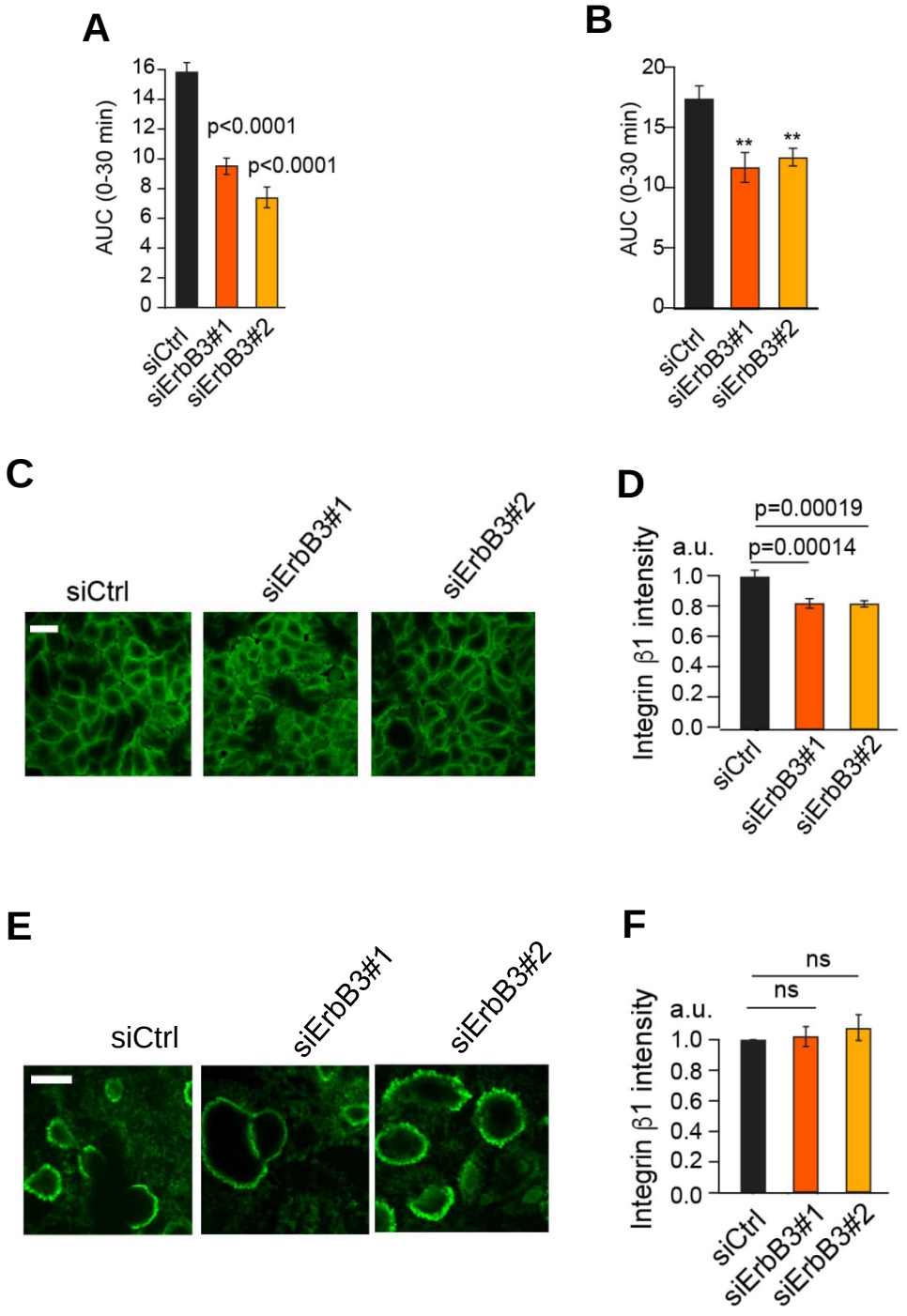

Suppl. Figure S2

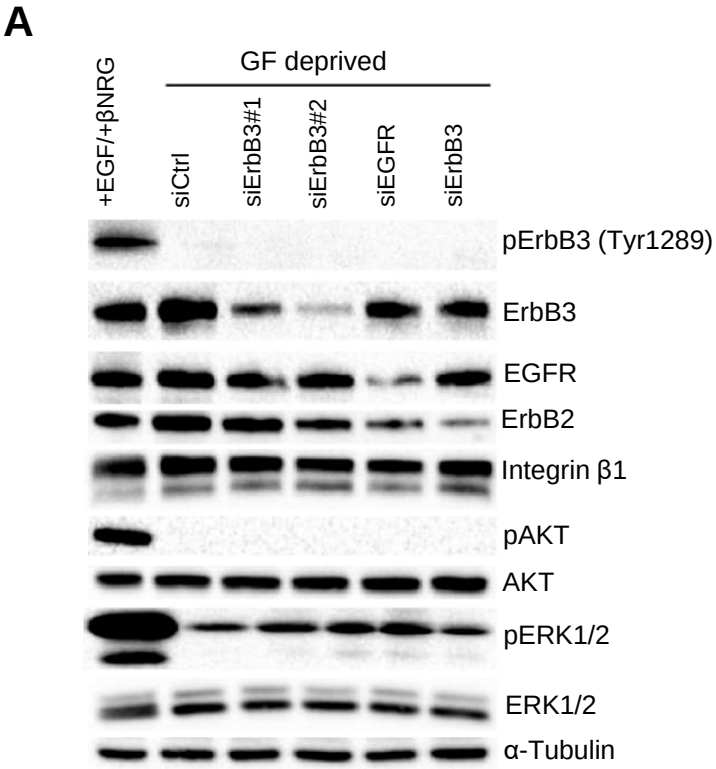

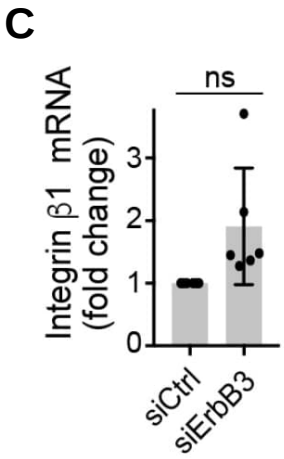

Suppl. Figure S3

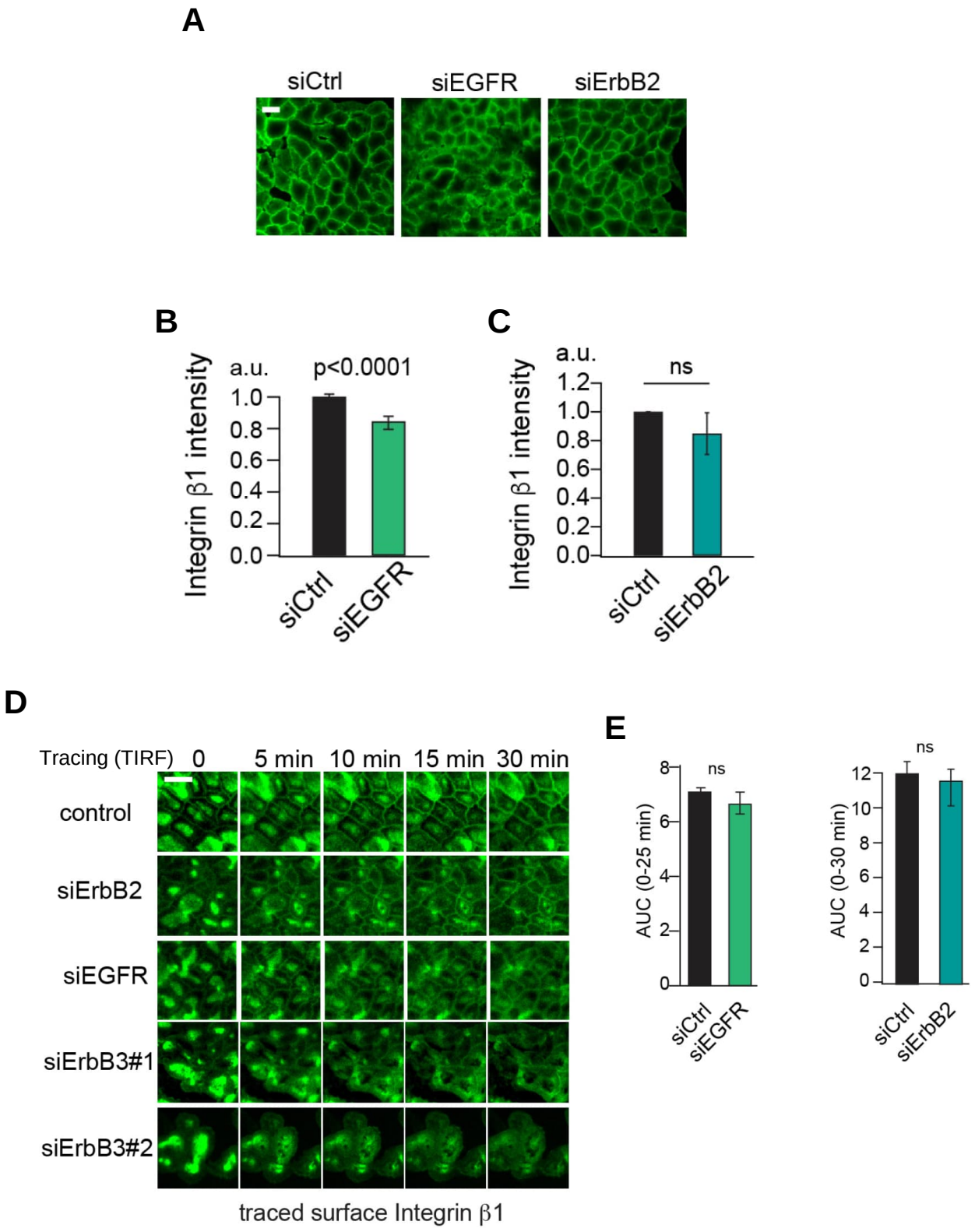

Suppl. Figure S4

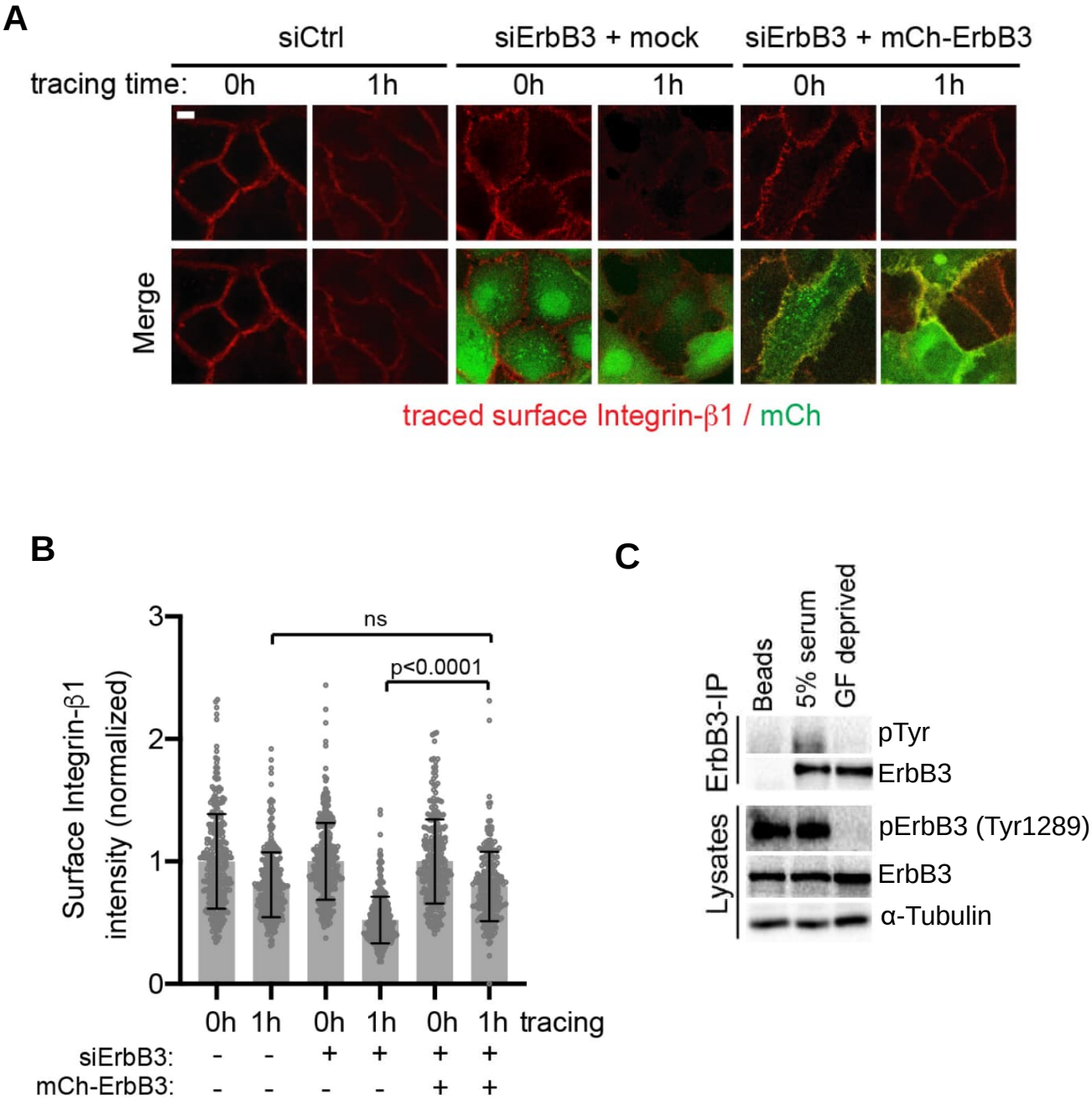

Suppl. Figure S5

A

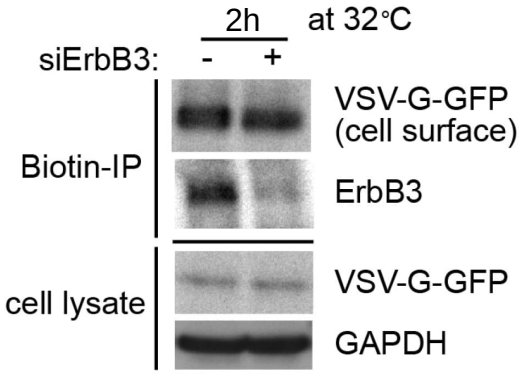

B

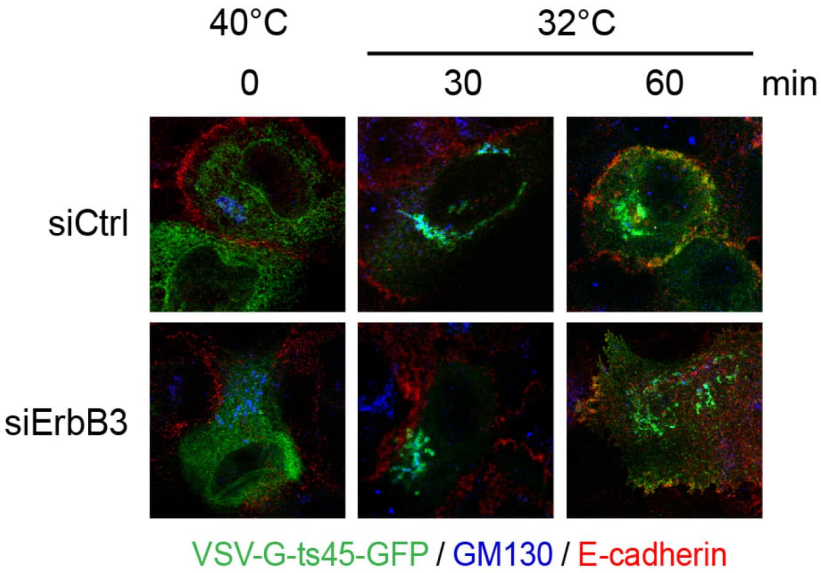

Suppl. Figure S6

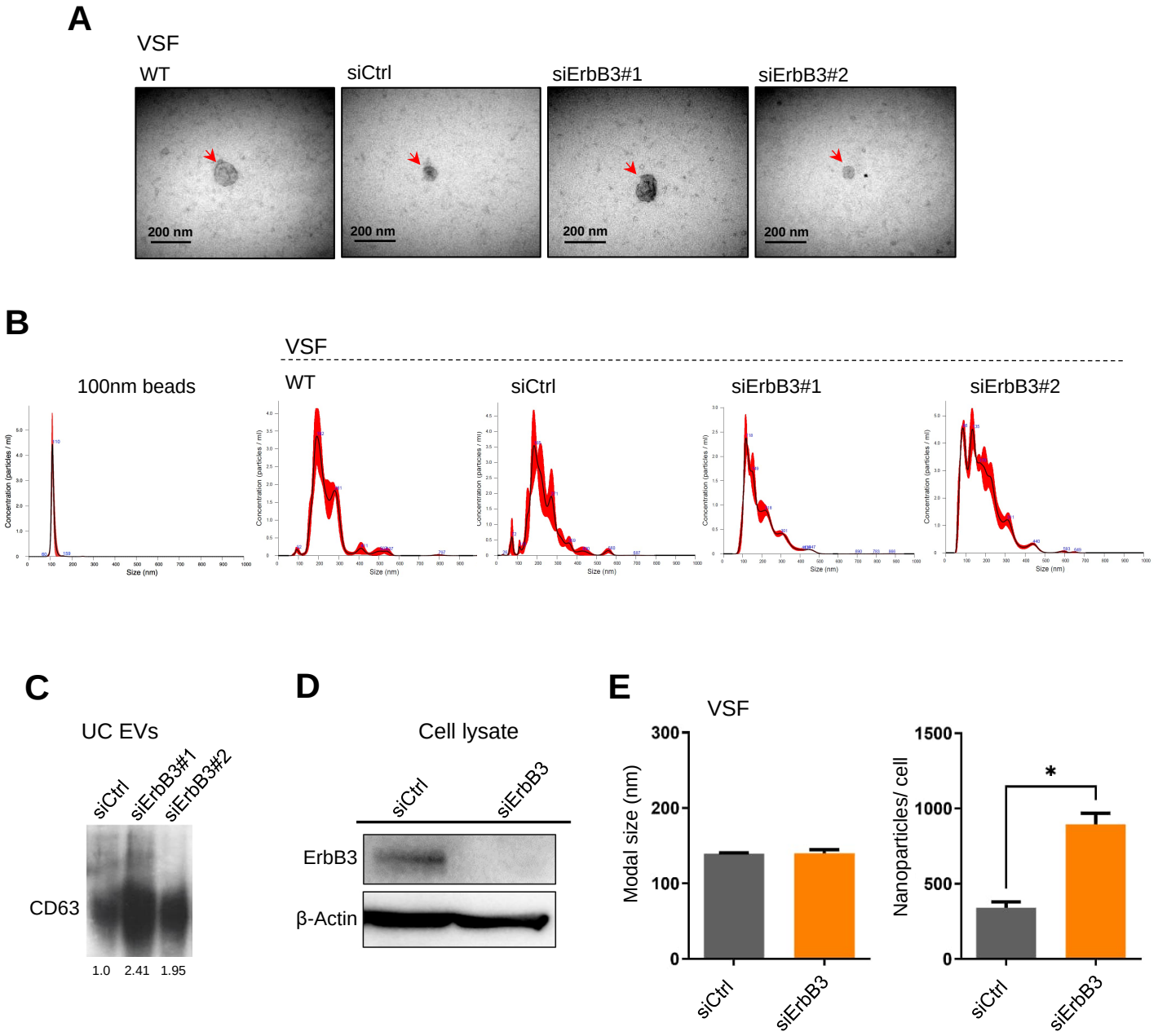

Suppl. Figure S7

A

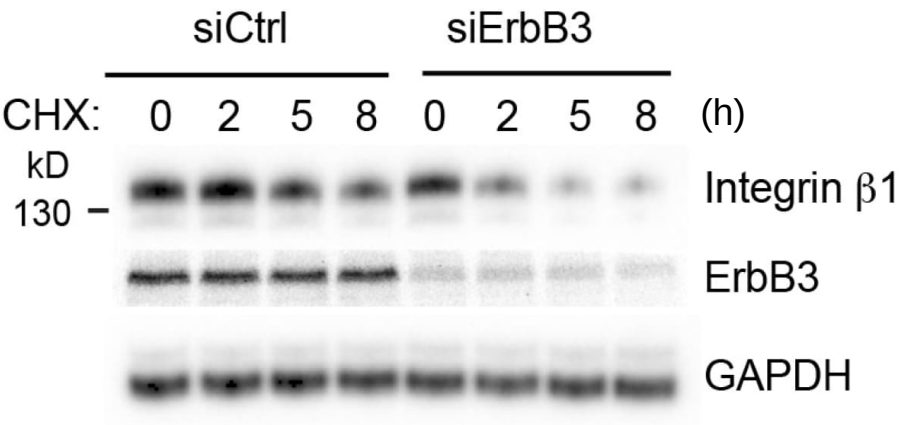

B

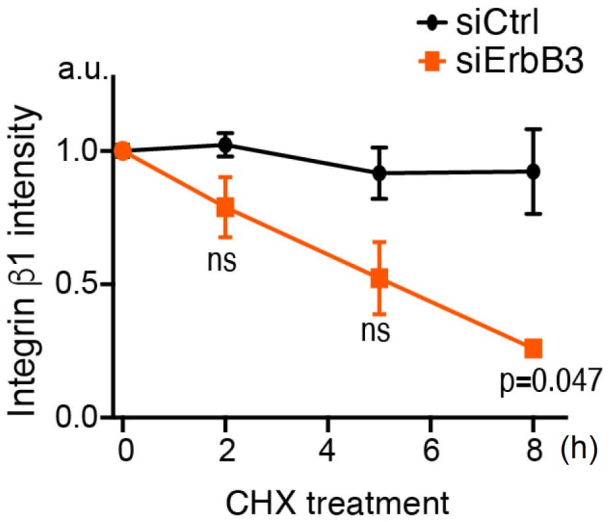

Suppl. Figure S8

A

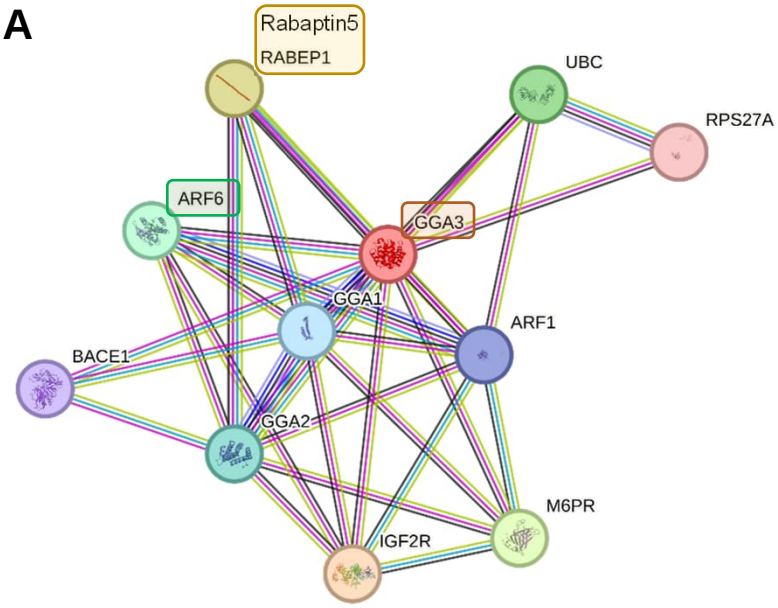

B

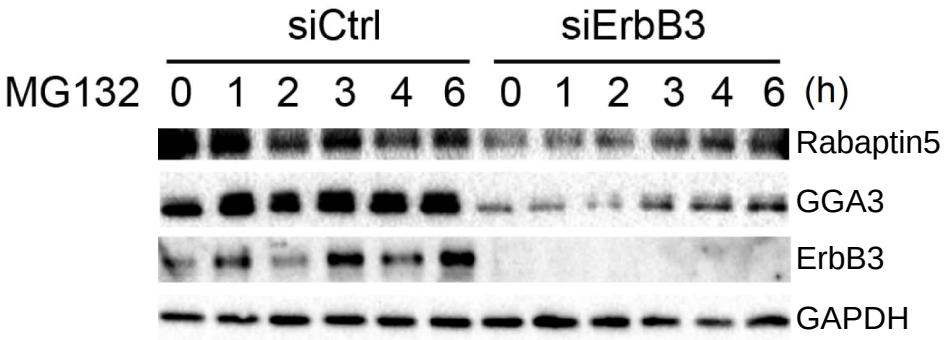

C

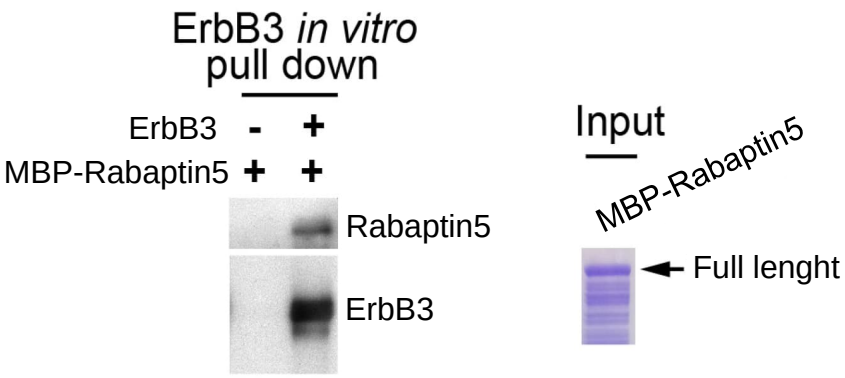

Suppl. Figure S9